Paleoceanography and Paleoclimatology

RESEARCH ARTICLE
10.1029/2020PA004095

Key Points:

- Southern Ocean winter water and sea ice extent can be reconstructed using the oxygen isotopic composition of planktonic and benthic foraminifera
- Summertime calcification of the planktonic foraminifer *N. pachyderma* likely occurs in sub-surface winter water
- Preliminary sea ice reconstruction for the late Holocene is consistent with satellite-base estimates in the Atlantic sector of the Southern Ocean

Supporting Information:

Supporting Information may be found in the online version of this article.

Correspondence to:

D. C. Lund,
david.lund@uconn.edu

Citation:

Lund, D. C., Chase, Z., Kohfeld, K. E., & Wilson, E. A. (2021). Tracking Southern Ocean sea ice extent with winter water: A new method based on the oxygen isotopic signature of foraminifera. *Paleoceanography and Paleoclimatology*, *36*, e2020PA004095. https://doi.org/10.1029/2020PA004095

Received 25 AUG 2020
Accepted 6 MAY 2021

Tracking Southern Ocean Sea Ice Extent With Winter Water: A New Method Based on the Oxygen Isotopic Signature of Foraminifera

David C. Lund[1], Zanna Chase[2], Karen E. Kohfeld[3,4], and Earle A. Wilson[5]

[1]Department of Marine Sciences, University of Connecticut - Avery Point, Groton, CT, USA, [2]Institute for Marine and Antarctic Studies, University of Tasmania, Hobart, TAS, Australia, [3]School of Resources and Environmental Management, Simon Fraser University, Burnaby, BC, Canada, [4]School of Environmental Science, Simon Fraser University, Burnaby, BC, Canada, [5]Division of Geological and Planetary Sciences, California Institute of Technology, Pasadena, CA, USA

Abstract Southern Ocean sea ice plays a central role in the oceanic meridional overturning circulation, transforming globally prevalent watermasses through surface buoyancy loss and gain. Buoyancy loss due to surface cooling and sea ice growth promotes the formation of bottom water that flows into the Atlantic, Indian, and Pacific basins, while buoyancy gain due to sea ice melt helps transform the returning deep flow into intermediate and mode waters. Because northward expansion of Southern Ocean sea ice during the Last Glacial Maximum (LGM; 19–23 kyr BP) may have enhanced deep ocean stratification and contributed to lower atmospheric CO_2 levels, reconstructions of sea ice extent are critical to understanding the LGM climate state. Here, we present a new sea ice proxy based on the $^{18}O/^{16}O$ ratio of foraminifera ($\delta^{18}O_c$). In the seasonal sea ice zone, sea ice formation during austral winter creates a cold surface mixed layer that persists in the sub-surface during spring and summer. The cold sub-surface layer, known as winter water, sits above relatively warm deep water, creating an inverted temperature profile. The unique surface-to-deep temperature contrast is reflected in estimates of equilibrium $\delta^{18}O_c$, implying that paired analysis of planktonic and benthic foraminifera can be used to infer sea ice extent. To demonstrate the feasibility of the $\delta^{18}O_c$ method, we present a compilation of *N. pachyderma* and *Cibicidoides* spp. results from the Atlantic sector that yields an estimate of winter sea ice extent consistent with modern observations.

Plain Language Summary Sea ice coverage in the Southern Ocean plays a critical role in Earth's climate system by influencing ocean-atmosphere gas exchange and the global ocean circulation. While satellite observations provide detailed information on sea ice cover in the modern era, the satellite record is only a few decades in duration, limiting our long-term perspective. An improved understanding of sea ice requires reconstructions in the geologic past under climate conditions different than today. Here, we propose a new technique for reconstructing sea ice extent in the Southern Ocean based on the $^{18}O/^{16}O$ ratio ($\delta^{18}O_c$) of foraminifera. The $\delta^{18}O_c$ of foraminifera is sensitive to temperature and it can therefore be used to infer areas of surface cooling where sea ice tends to form and warmer areas where sea ice melts. We present an initial compilation of data showing that the $\delta^{18}O_c$ method yields an estimate of modern sea ice extent consistent with satellite observations, highlighting the potential of the $\delta^{18}O_c$ method for paleoclimate studies.

1. Introduction

Southern Ocean sea ice plays an important role in air-sea exchange of CO_2 and the ocean's overturning circulation. Expanded sea ice coverage during the Last Glacial Maximum (LGM; 19–23 kyr BP) may influence atmospheric CO_2 directly, by blocking air-sea gas exchange (Morales Maqueda & Rahmstorf, 2002; Stephens & Keeling, 2000; Watson et al., 2015) and indirectly, by promoting brine formation and the global expansion of Antarctic Bottom Water (AABW) (Adkins et al., 2002; Jansen & Nadeau, 2016). As the upper boundary of AABW shoals and moves away from the zone of intense mixing near the seafloor, reduced mixing with overlying watermasses will tend to isolate abyssal waters and promote oceanic carbon sequestration (Adkins, 2013; De Boer & Hogg, 2014; Lund et al., 2011; Marzocchi & Jansen, 2019). Additionally, greater sea ice growth, transport, and melt could enhance the meridional overturning circulation, decrease the residence time of surface waters in the Southern Ocean, and further limit equilibration of the deep ocean inorganic carbon pool with the atmosphere (Eggleston & Galbraith, 2018; E. D. Galbraith & Skinner, 2020; Khatiwala et al., 2019; Haumann et al., 2016). A clear picture of Southern Ocean sea ice cover is therefore essential to understand the mechanisms that drive glacial-interglacial climate change.

Previous sea ice reconstructions have been based on several proxies, including: sediment lithology (Burckle & Cirilli, 1987; Burckle & Mortlock, 1998; Burckle et al., 1982; Hays et al., 1976), diatom assemblages (Allen et al., 2011; Benz et al., 2016; Collins et al., 2012; Crosta et al., 1998; DeFelice, 1979; Gersonde et al., 2003, 2005), chemical tracers in ice cores (ssNa, Br, MSA; Abram et al., 2013; Thomas et al., 2019), and highly branched isoprenoid alkenes (e.g., Belt, 2018; Belt et al., 2016; Collins et al., 2013; Massé et al., 2011; Vorrath et al., 2019). The most extensive maps of Southern Ocean sea ice are based on sea-ice indicator diatom species (Gersonde et al., 2003) and/or statistical models using diatom assemblage-based transfer functions (Benz et al., 2016; Crosta et al., 1998; Ferry et al., 2015; Gersonde et al., 2005; Whitehead & McMinn, 2002). These proxies provide important insights into past sea-ice distributions, but like all proxies, they can be affected by issues such as non-analog situations (Crosta et al., 2004), selective dissolution (Burckle, 1983; Gersonde & Zielinski, 2000; Pichon et al., 1992), and core top calibration uncertainty (Esper & Gersonde, 2014; Esper et al., 2010). The use of multiple proxies, especially those based on independent approaches (e.g., Kucera et al., 2005; Peck et al., 2015), is beneficial for painting a more complete picture of past changes in sea ice.

Here, we present a novel technique for reconstructing Southern Ocean sea ice extent (SIE) using the oxygen isotopic signature ($\delta^{18}O_c$) of foraminifera. Our method is based on the observed spatial distribution of winter water (WW), a cold near-surface layer that overlies warmer Circumpolar Deep Water (CDW) and persists beneath the seasonal pycnocline during austral summer. If planktonic foraminifera secrete their calcite in or near equilibrium with WW, the resulting $\delta^{18}O_c$ should be heavier than co-located benthic $\delta^{18}O_c$. Beyond the reach of WW, planktonic $\delta^{18}O_c$ should be similar to or lighter than benthic $\delta^{18}O_c$ because the weaker halocline and stronger surface warming maintain a water column with less pronounced subsurface temperature inversions (Pellichero et al., 2017). As a result, we propose that meridional transects of planktonic and benthic $\delta^{18}O_c$ can be used to map relative changes in WW and winter sea ice (WSI) extent in the Southern Ocean. Our method builds on the work of Matsumoto et al. (2001), who used latitudinal trends in planktonic and benthic $\delta^{18}O_c$ to infer the position of the Polar Front.

The remainder of the paper is organized as follows. First, in the background section, we briefly review the role of sea ice in Southern Ocean watermass transformation processes and the LGM climate state. Next, in the method rationale section, we discuss the spatial extent of WW in the Southern Ocean, its relationship to sea ice, and how sea ice extent can be inferred using the $\delta^{18}O_c$ of foraminifera. Finally, in the results section, we present a compilation of published Holocene data from the Atlantic sector of the Southern Ocean to show that $\delta^{18}O_c$ results yield an estimate of WSI extent consistent with modern observations. We also show preliminary data for the LGM and discuss strategies for improving sea ice estimates during this time interval.

2. Background

2.1. Role of Sea Ice in Southern Ocean Watermass Transformation

Sea ice plays a central role in the transformation of watermasses in the Southern Ocean, where persistent surface westerly winds and Ekman divergence drive upwelling of deep waters from the Atlantic, Indian, and Pacific basins along isopycnal surfaces toward Antarctica. As deep waters are entrained into the Antarctic Circumpolar Current, they mix to form CDW, the predominant watermass in the Southern Ocean (Talley, 2013; Whitworth & Nowlin, 1987). Lower CDW is characterized by a salinity maximum, due to the influence of high salinity North Atlantic Deep Water (Figure 1) (Whitworth & Nowlin, 1987). As CDW upwells toward the surface, it diverges into a southward flowing lower branch and northward flowing upper branch. In the lower branch, surface buoyancy loss due to cooling, sea ice formation, and brine rejection transforms CDW into AABW (Naveira Garabato et al., 2002; Talley, 2013; Vernet et al., 2019; Whitworth & Nowlin, 1987). In the upper branch, surface buoyancy gain due to sea ice melt, precipitation, and surface

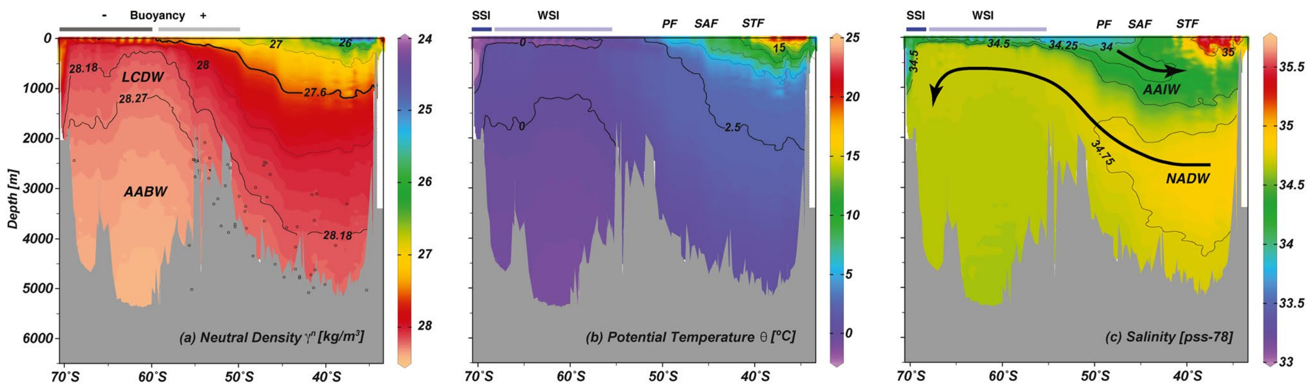

Figure 1. WOCE A12/S2 hydrographic sections at the approximate longitude of Atlantic sector oxygen isotope results (20°E to 20°W). (a) Neutral density section, including the 27.6 kg m^{-3} isopycnal (thick black line) that marks the dividing line between positive and negative surface buoyancy forcing regimes (Pellichero et al., 2018). Surface waters north of the line are subject to positive buoyancy fluxes (light gray horizontal bar) while surface waters to the south are subject to negative buoyancy fluxes (dark gray horizontal bar). Also noted are Lower Circumpolar Deep Water (LCDW) and Antarctic Bottom Water (AABW), as defined by neutral density surfaces (thin black lines) (Orsi et al., 1999). (b) Potential temperature section, including the approximate locations of the Polar Front (PF), Sub-Antarctic Front (SAF), and Subtropical Front (STF) at ∼50°S, 46°S, and 40°S, respectively (Belkin & Gordon, 1996). Approximate summer sea ice (SSI) extent and winter sea ice extent (WSI) are shown as blue horizontal bars on the upper *x*-axis (http://nsdic.org). (c) Salinity section for WOCE A12/S2, showing low salinity AAIW and high salinity NADW.

warming transforms CDW into Sub-Antarctic Mode Water (SAMW) and Antarctic Intermediate Water (AAIW) (Abernathey et al., 2016; Orsi et al., 1995; Pellichero et al., 2018; Saenko et al., 2002). The seasonal cycle of sea ice acts as a buoyancy pump that removes freshwater from the Antarctic margin, promoting AABW production, and adds freshwater along the sea ice edge, facilitating AAIW formation (Pellichero et al., 2018).

2.2. Winter Sea Ice Extent During the Last Glacial Maximum

Early reconstructions of Southern Ocean sea ice for the LGM were based on the lithology of seafloor sediments. Reconstructions by the CLIMAP (Climate: Long-range Investigation, Mapping And Prediction) project relied on the latitudinal boundary between diatom ooze and less diatomaceous radiolarian clays, where clay deposition was interpreted to represent perennial sea ice cover, that is, the northern edge of summer sea ice (Burckle et al., 1982; CLIMAP Project Members, 1976; Hays et al., 1976). The winter sea ice edge was estimated as the half-way point between the summer sea ice edge and the Polar Front, which was identified using faunal indicators (CLIMAP Project Members, 1976). The available lithological data implied that the LGM winter sea ice edge in the Atlantic sector (30°W to 30°E) was located at 49 ± 2°N, or ∼5° north of its current position.

More recently, sea ice indicator diatoms have become the primary proxy for sea ice extent. One common approach involves using the relative abundance of *F. curta* and *F. cylindrus* in core top sediments, which has been shown to correspond with the modern WSI edge (Gersonde & Zielinski, 2000). While there is little discernible relationship between sea ice conditions and the flux of *F. curta* and *F. cylindrus* to sediment traps, within ±2° of the ice edge their combined abundance in sediment core tops ranges from 3% to 15% of the total diatom assemblage (Gersonde & Zielinski, 2000; Zielinski & Gersonde, 1997). Given that diatom flux to the sediments is minimal during intervals of sea ice cover, the abundance signal likely reflects the integrated effect of repeated sea-ice advance and retreat over many years (Gersonde & Zielinski, 2000). Using the abundance of *F. curta* and *F. cylindrus* in well-dated sediment cores, Gersonde et al. (2003) estimated maximum winter SIE from 30°W to 30°E reached 48 ± 1°S during the LGM, roughly 6° north of its current position. Crosta et al. (1998) reached a similar conclusion by applying the modern-analog technique to diatom assemblages, although the reconstructed winter ice extent showed somewhat greater latitudinal variability (48 ± 2°S). A more recent study by Allen et al. (2011) also suggests LGM winter SIE expanded ∼5° northward in the Scotia Sea. Because *F. curta* and *F. cylindrus* are vulnerable to selective dissolution, the diatom-based techniques depend on moderate to high sediment preservation and reasonably high opal fluxes (Burckle, 1983; Gersonde & Zielinski, 2000).

Phylogenetic patterns in bull kelp have also been used to estimate SIE in the Southern Ocean. Because bull kelp cannot survive along coastlines influenced by ice scour, the retreat of sea ice allows for recolonization, which can be traced using kelp DNA. Sub-Antarctic islands with the least genetically diverse kelp specimens correspond approximately with the diatom-inferred location of the LGM WSI edge (Fraser et al., 2009). In the Indian Ocean sector, however, the bull kelp results suggest that WSI extended several degrees further northward than indicated by the limited available diatom-based constraints (Fraser et al., 2009). In the Atlantic sector, the two methods agree within ∼±2°, which is similar to the difference between existing diatom-based reconstructions (Allen et al., 2011; Crosta et al., 1998; Gersonde et al., 2003).

2.3. Implications for LGM Climate

Greater sea ice cover in the Southern Ocean may have contributed to lower atmospheric CO_2 levels during the LGM. Nearly the entire atmospheric pCO_2 decline can be achieved if >99% of the area south of the modern Polar Front was covered in sea ice year-round (Stephens & Keeling, 2000). This is the maximum possible effect, however, because: (1) modern observations indicate that the area of open water within the sea ice pack ranges from 20% to 30% (Watkins & Simmonds, 1999), and (2) summer sea ice during the LGM does not appear to have extended to the Polar Front (Gersonde et al., 2005). A more realistic value for sea ice coverage of 75% yields a much smaller CO_2 signal of ∼15 ppm, or ∼20% of the glacial-interglacial signal (Stephens & Keeling, 2000). The effectiveness of sea ice in blocking air-sea gas exchange is limited because greater areal coverage results in higher surface ocean dissolved inorganic carbon concentrations, which enhances the air-sea CO_2 gradient, thereby driving greater outgassing in areas of open water (Morales Maqueda & Rahmstorf, 2002). Sea ice also weakens the biological pump by decreasing light availability, an effect that further offsets the physical blocking effect (Gupta et al., 2020; Sun & Matsumoto, 2010).

In addition to acting as a physical barrier to gas exchange, sea ice may influence outgassing of CO_2 by altering the location and rate of overturning in the Southern Ocean. Northward expansion of the seasonal sea ice zone would mean that surface waters south of the Ekman divergence are exposed at the surface for a longer period of time (Watson et al., 2015). Assuming slower vertical overturning and no light or iron limitation, the increase in surface water residence time would drive greater nutrient consumption, lower preformed nutrients, and therefore greater transfer of carbon into the ocean interior by the biological pump (Watson et al., 2015). Alternatively, expanded sea-ice cover may accelerate the meridional overturning, which would enhance the existing air-sea disequilibrium and limit oceanic outgassing of CO_2 (Galbraith & de Lavergne, 2019; Galbraith & Skinner, 2020; Saenko et al., 2002; Stössel et al., 1998; Khatiwala et al., 2019). To further complicate matters, the horizontal circulation in the Southern Ocean must also be considered because it mediates the accumulation of respired carbon in subpolar gyres, which in turn influences the air-sea CO_2 gradient (MacGilchrist et al., 2019). During the LGM, sea ice cover may inhibit export production in subpolar gyres, reducing the accumulation of respired carbon in CDW, counteracting enhanced carbon storage due to other factors.

Sea ice may also influence atmospheric CO_2 via the deep ocean stratification, which reflects integrated buoyancy loss around Antarctica. If the area of negative buoyancy forcing around Antarctica expanded ∼5° northward during the LGM and the slope of isopycnals in the Antarctic Circumpolar Current remained similar to today, the density surface acting as the upper "lid" for AABW would have shoaled (Ferrari et al., 2014). Once the upper boundary of AABW has moved away from the zone of intense mixing near the seafloor, vertical mixing between southern and northern water masses would decrease, allowing for carbon to accumulate in the abyss (Adkins, 2013; Lund et al., 2011). Shoaling can occur by either expanding the zone of negative surface buoyancy flux or by increasing the buoyancy loss rate over a smaller region (Jansen & Nadeau, 2016). At steady state, buoyancy loss around Antarctica must be balanced by diffusive buoyancy flux between the lower and upper overturning cells (Jansen & Nadeau, 2016). Thus, greater sea ice formation in the Southern Ocean causes contraction of NADW as its properties are modified by mixing with AABW (Jansen & Nadeau, 2016).

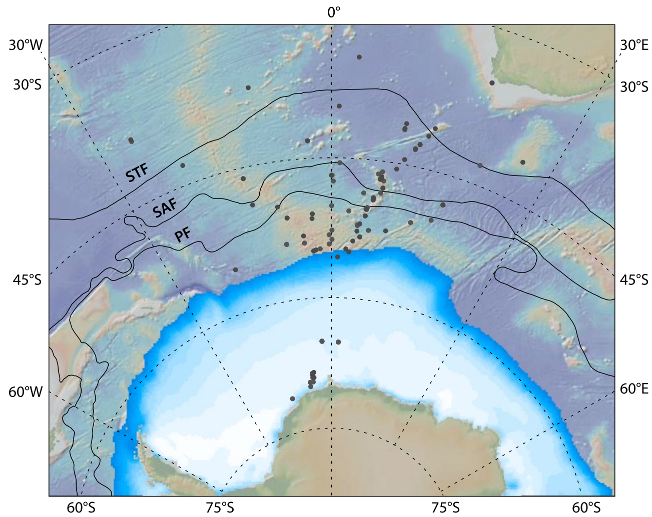

Figure 2. Mean Southern Ocean sea ice concentration for September 1979-2007 (http://nsdic.org) contoured at 5% intervals. Darkest blue shading represents >15% sea ice concentration, white represents 100%. Also included is the approximate location of key Southern Ocean fronts, including the subtropical front (STF), sub-Antarctic Front (SAF), and Polar Front (PF) (from Orsi et al., 1995). Core locations for published $\delta^{18}O_c$ results in Figure 8 are shown as circles. Map generated using GeoMapApp (Ryan et al., 2009).

3. Method Rationale

Given the myriad ways that Southern Ocean sea ice can influence the oceanic circulation, reconstructions of sea ice extent are an essential component of any effort to understand glacial-interglacial CO_2 cycles. Below, we outline a new method to constrain sea ice extent that involves mapping winter water (WW) using the oxygen isotopic signature of foraminifera. The following text includes a brief description of the study area followed by discussion of WW and its relation to sea ice extent. We then discuss the influence of surface cooling on the $\delta^{18}O$ of calcite ($\delta^{18}O_c$) and the depth habitat of the planktonic foraminifer (*N. pachyderma*) that likely records the WW $\delta^{18}O_c$ signal.

3.1. Winter Sea Ice Extent in the Study Area

Our study focuses on the Atlantic sector of the Southern Ocean, in particular 20°W to 20°E, where there is an existing array of Holocene foraminiferal $\delta^{18}O_c$ data that straddle the modern WSI edge (Figure 2). By convention, the ice edge is defined as the 15% ice concentration contour inferred from satellite observations (Hobbs et al., 2016). The ice concentrations depicted in Figure 2 represent climatological values for September, when sea ice is at its greatest extent. The climatological WSI edge varies by ±1° latitude across the study area, facilitating the comparison between modern observations and $\delta^{18}O_c$-based reconstructions. East of 25°E, however, the WSI edge is located several hundred kilometers to south, highlighting the spatially heterogeneous nature of ice cover in the Southern Ocean (Figure 2). Satellite observations also show that the winter ice edge at any given location varies by ±2° on an interannual basis (www.nsidc.org). Thus, we should expect a latitudinal precision of no better than ±2° for paleo-reconstructions.

3.2. Winter Water and Sea Ice Extent

Wintertime cooling in the Southern Ocean causes surface buoyancy loss and the creation of a cold surface mixed layer. In the seasonal sea ice zone, ice formation and brine rejection create a mixed layer characterized by temperatures below −1.5°C (Martinson, 1990; Pellichero et al., 2017; Wilson et al., 2019). Between the seasonal sea ice zone and the Polar Front, the mixed layer temperature is warmer, ranging from −1.5°C to 1.5°C (Pellichero et al., 2017). During spring and summer, enhanced solar insolation and ice melt creates a relatively warm and fresh surface layer that caps the winter mixed layer, leaving a cold sub-surface remnant known as WW (Moffat & Meredith, 2018; Sabu et al., 2020). The summertime vertical temperature profile is therefore characterized by warm-cold-warm layering, with the WW layer typically occupying the depth range from 50 to 200 m (Figure S1).

To evaluate the spatial relationship between WW and WSI, we use summertime (January–May) WOCE sections to determine the latitude of WW isotherms in the 50–150 m depth range. As discussed below, this depth range overlaps with the habitat of the planktonic foraminifer *N. pachyderma*. The latitude of WW isotherms was compared to the climatological WSI extent for 1979–2019 and to the sea ice extent during the September prior to the corresponding WOCE section (www.nsidc.org). At the warm end of the WW spectrum, we find that the 1°C isotherm is located on average 3° north of the WSI edge; at the cold end, the −1.5°C WW isotherm falls on average 4° to the south (Figure 3). The best match between WSI and WW spatial extent occurs for the −0.5°C and 0°C isotherms, which are on average located within 1° of the ice edge. The correspondence between WSI and WW is insensitive to whether ice extent is defined using climatological values or those from the prior September. Compared to the ~10° latitudinal range in WSI extent, the spatial offset between WW isotherms and the ice edge is small, implying that relative changes in the latitude of WW isotherms can be used to track WSI.

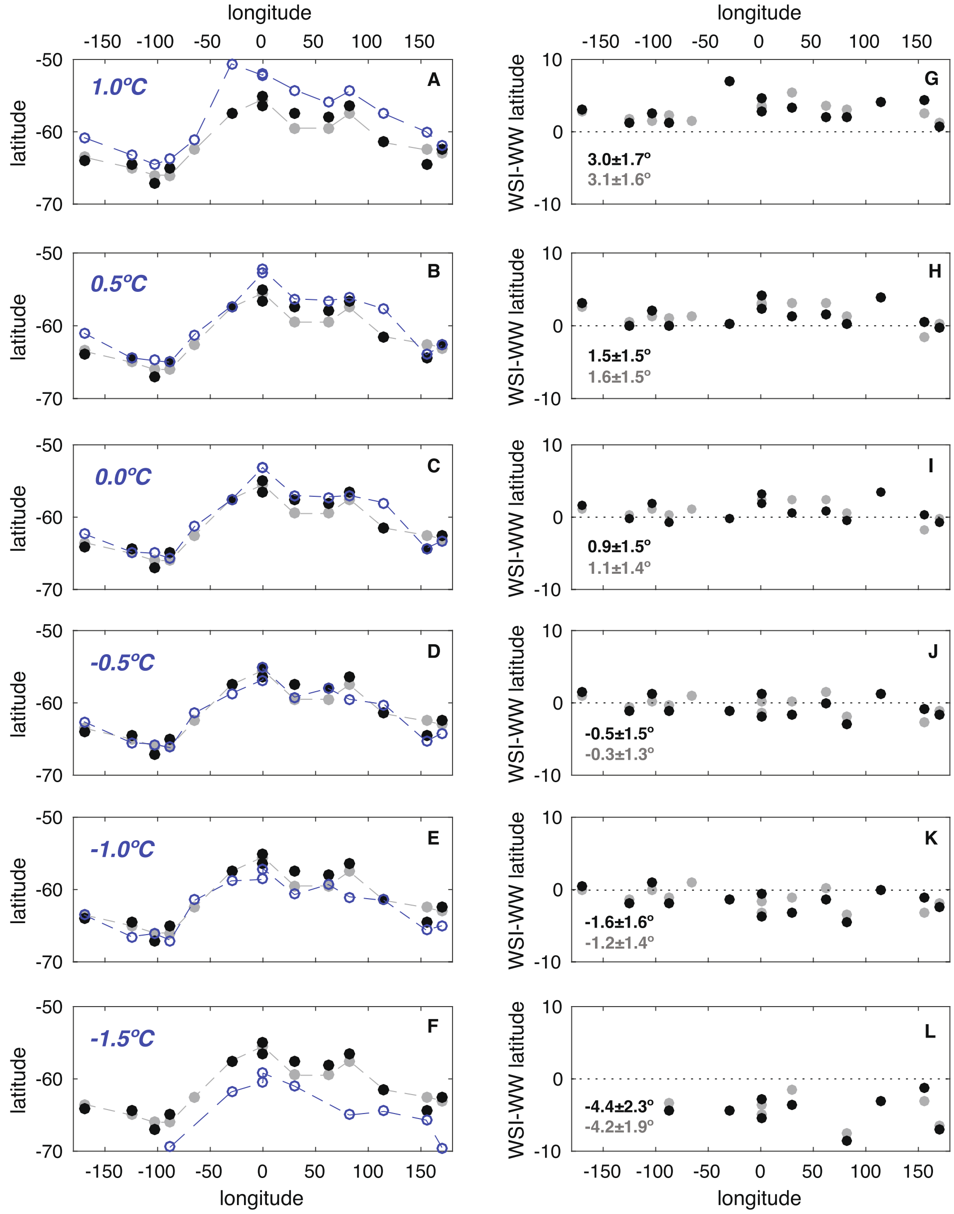

Figure 3. Latitude of winter water (WW) isotherms relative to the winter sea ice (WSI) edge in the Southern Ocean. (a) Latitude of the 1.0°C WW isotherm (open blue circles) versus longitude, determined using 14 summertime WOCE hydrographic sections and the depth habitat range of *N. pachyderma* (50–150 m). Also shown is the sea ice edge the September prior to the corresponding hydrographic section (black circles) and the climatological WSI edge from 1981 to 2010 (gray circles). The WSI edge was determined using September satellite observations from 1981 to 2020 (http://nsdic.org). (b–f) Same as panel A, but for WW isotherms of 0.5°C, 0.0°C, −0.5°C, −1.0°C, and −1.5°C. (g) WSI latitude minus WW latitude for the 1.0°C isotherm. On average, the 1.0°C isotherm is found 3.0±1.7° north of the prior September ice edge (black circles) and 3.1±1.6° north of the climatological WSI edge (gray circles). In each case, the stated error is 1σ; the standard errors are ~4x lower. (h–l) Same as panel G, but for WW isotherms of 0.5°C, 0.0°C, −0.5°C, −1.0°C, and −1.5°C. The best match between WW and WSI latitudes occurs for the −0.5°C isotherm (J).

To cross-check the results in Figure 3, we also mapped WW isotherms using the Monthly Isopycnal & Mixed-layer Ocean Climatology (MIMOC) and Roemmich-Gilson (RG) gridded data products. The MIMOC product is a global climatology based on conductivity-temperature-depth (CTD) data from Argo floats, shipboard casts, and ice-tethered profilers (Schmidtko et al., 2013). Since the MIMOC product excludes a large portion of Southern Ocean Argo float data collected since 2012, we compare these climatological values with those from the objectively mapped RG Argo climatology, which spans January 2004 to December 2020

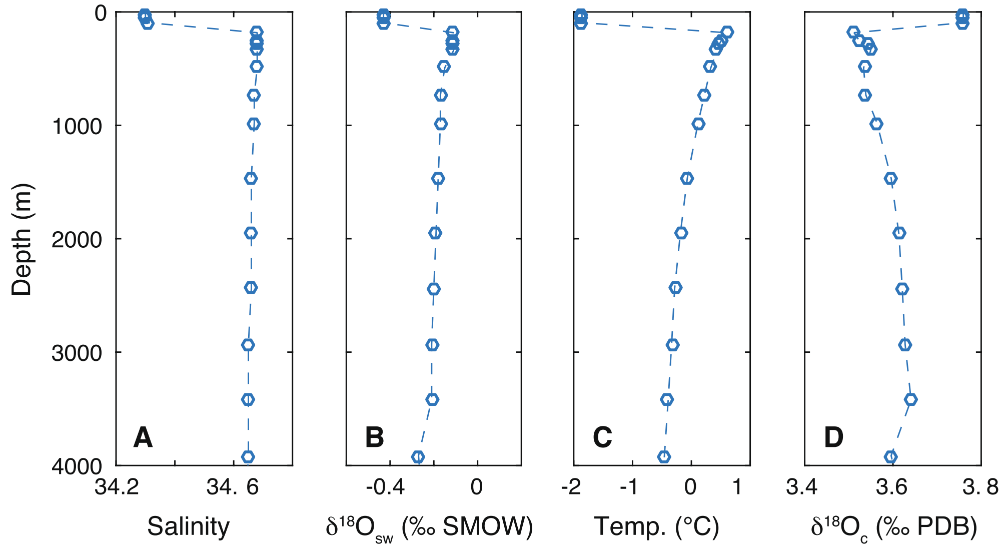

Figure 4. Vertical hydrographic profiles at 1°E, 61°S from October 1989 (Mackensen et al., 1996), including (a) salinity, (b) $\delta^{18}O_{sw}$ (SMOW), (c) in situ temperature, and (d) the calculated equilibrium $\delta^{18}O$ of calcite ($\delta^{18}O_c$) (PDB). $\delta^{18}O_c$ was determined using the quadratic equation for *Cibicidoides spp*., calibrated using data from −1°C to 25°C (Marchitto et al., 2014). The Marchitto et al. (2014) core top calibration yield a ($\delta^{18}O_c$–$\delta^{18}O_{sw}$) versus T relationship that is indistinguishable from the inorganic precipitation experiments of Kim and O'Neil (1997).

(Roemmich & Gilson, 2009). The RG climatology extends to a southernmost latitude of 65°S. The JFM climatology for each product is shown in Figure S2. Similar to the WOCE results in Figure 3, the maps show that WW isotherms parallel WSI extent throughout the Southern Ocean. Offsets between the 0°C isotherm and the ice edge are generally less than 2°, particularly from ~10°W to 30°E and ~130°W to 70°W. In areas where fronts are constricted by bathymetry, near 60°W and 150°E, the offsets are larger. For example, at 56°W, the 0°C WW isotherm is located at ~58°S, or ~4° north of the WSI edge (Cunningham et al., 2003). The reason for the spatial decoupling at this location is unclear, but it may be related to the focused flow of the ACC through Drake Passage. To first order, however, the spatial offset between WW isotherms and WSI in the Southern Ocean is small relative to the total latitudinal range in sea ice extent, supporting the idea that WSI can be mapped using WW.

3.3. Influence of Surface Cooling on the $\delta^{18}O$ of Calcite

The unique hydrography of the Southern Ocean is reflected in vertical profiles of the $\delta^{18}O$ of calcite ($\delta^{18}O_c$), which is a function of both the $\delta^{18}O$ of seawater ($\delta^{18}O_{sw}$) and temperature. As an example, we use a profile from 1°E, 61°S that is representative of wintertime conditions in the seasonal sea ice zone. The salinity profile displays a strong halocline due to surface freshening (Figure 4a). Similarly, the $\delta^{18}O_{sw}$ profile shows a small surface depletion but otherwise shows only minor variations below 200 m (Figure 4b). Temperatures are near freezing (−1.8°C) in the upper 150 m and systematically warmer (~0°C) from 1,000 to 4,000 m (Figure 4c). The influence of the winter mixed layer is evident in the vertical profile of $\delta^{18}O_c$ where temperature-dependent fractionation overwhelms the small surface depletion in $\delta^{18}O_{sw}$, yielding surface $\delta^{18}O_c$ values that are greater than those deeper in the water column (Figure 4d). Surface cooling therefore creates a unique vertical $\delta^{18}O_c$ profile, which reflects the winter mixed layer positioned over relatively warm deep waters.

To facilitate comparison with planktonic and benthic foraminiferal results, the inverted $\delta^{18}O_c$ profile in Figure 4 can be expressed as the difference between surface and deep $\delta^{18}O_c$. The surface (0–150 m) minus deep (1,500–3,500 m) $\delta^{18}O_c$ difference ($\Delta\delta^{18}O_c$) at 61°S is 0.2–0.3‰. Additional wintertime data from the same transect show a similar pattern, with positive $\Delta\delta^{18}O_c$ values spanning from 70°S to 54°S, the northernmost profile in the transect (Figure 5a). For this section, which is the only available wintertime section in our study area, the zone of positive $\Delta\delta^{18}O_c$ coincides with the northward extent of winter sea ice (WSI).

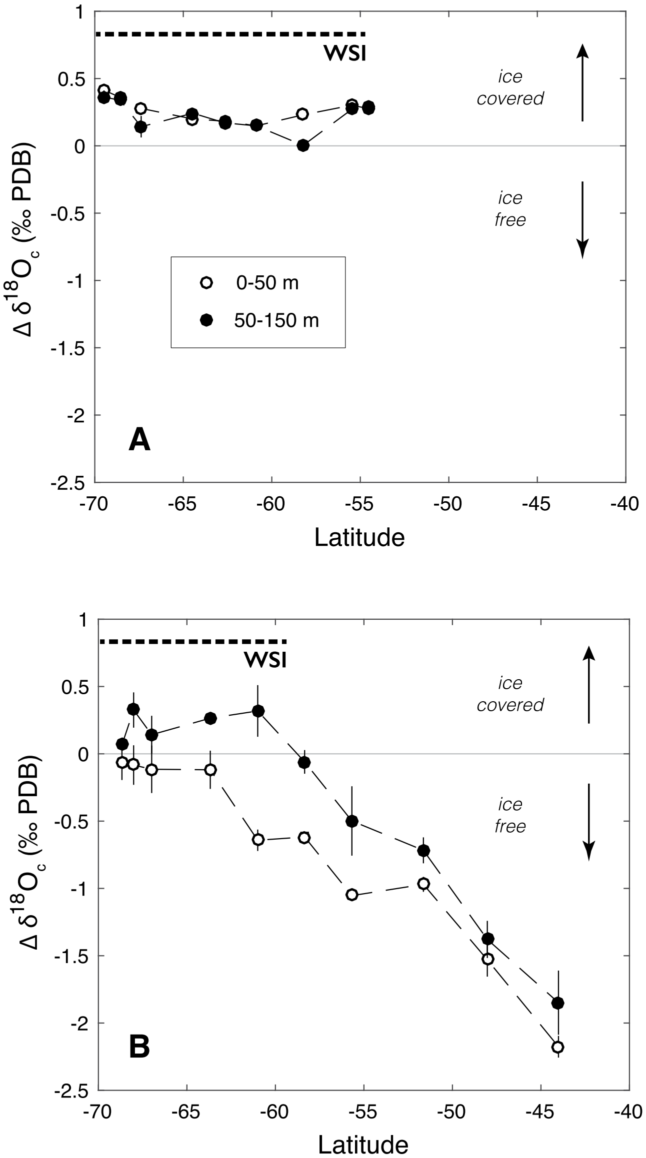

Figure 5. Predicted surface minus deep (1,500–3,500 m) $\delta^{18}O_c$ ($\Delta\delta^{18}O_c$) versus latitude. (a) $\Delta\delta^{18}O_c$ for austral winter near 0°E, using values from 0 to 50 m (open circles) and 50–150 m (closed circles). Error bars represent the propagated standard error for the mean surface and deep $\delta^{18}O_c$ at each location. On average, 2–4 individual $\delta^{18}O_c$ estimates were used to calculate the mean $\delta^{18}O_c$ for each depth range. Also shown is the average position of winter sea ice extent at 0°E (Figure 3). Positive $\Delta\delta^{18}O_c$ values correspond to regions of sea ice formation. Both $\Delta\delta^{18}O_c$ definitions yield similar results during austral winter. (b) Same as top panel but for austral summer at 30°E. Unlike at 0°E, the estimates of $\Delta\delta^{18}O_c$ diverge because surface warming yields lower $\delta^{18}O_c$ from 0 to 50 m. The $\Delta\delta^{18}O_c$ estimate based on sub-surface values corresponds with winter sea ice extent because temperatures from 50 to 150 m reflect the presence of remnant WW.

The influence of temperature on $\delta^{18}O_c$ is also apparent during austral summer. To illustrate this point, we use temperature and $\delta^{18}O_{sw}$ profiles from 30°E in the Southern Ocean collected during March 1993 (Archambeau et al., 1998). This is the closest transect to our study area that spans the entire latitude range of interest (~70°S to 40°S). To first order, the summer and winter temperature profiles look very similar in the seasonal sea ice zone, with both having the inverted pattern of cold over warm waters (Figure 6). But surface warming during austral summer creates a thin mixed layer above WW, resulting in a warm-cold-warm layering that is typical of austral summer conditions in the seasonal sea ice zone (Gordon & Huber, 1984; Pellichero et al., 2017; Wilson et al., 2019). The presence of WW from ~50 to 150 m yields equilibrium $\delta^{18}O_c$ values that are higher than in either the thin surface mixed layer or the underlying deep water. In the Polar Frontal Zone, between ~55°S and 48°S, the lack of WW yields a temperature profile that is nearly isothermal, but with a thin warm layer at the surface. Both features are reflected in the corresponding $\delta^{18}O_c$ profile. Moving further north into the sub-Antarctic Zone, between ~48°S and 42°S, a more traditional open water thermocline develops, which is characterized by warm (~10°C) surface waters positioned over CDW (Figure 6). As a result, the sub-Antarctic $\delta^{18}O_c$ profile shows surface ocean values that are 1–2‰ lower than those associated with CDW.

The presence of cold WW along the 30°E transect can be mapped using $\Delta\delta^{18}O_c$. Surface (0–50 m) minus deep (1,500–3,500 m) $\delta^{18}O_c$ values at 30°E are ~0‰ from 70°S to 64°S (Figure 5b), which reflects similar temperatures in the thin summer layer and deep waters. However, if we instead estimate $\Delta\delta^{18}O_c$ using hydrographic data from 50 to 150 m, which coincides with the WW layer, we observe positive $\Delta\delta^{18}O_c$ as far north as ~60°S, which is the approximate latitude of the WSI edge at 30°E (Figure 5b). Thus, $\Delta\delta^{18}O_c$ calculated using austral summer hydrographic data from 50 to 150 m reflects the influence of sea ice formation during the preceding winter, implying that planktonic and benthic $\delta^{18}O_c$ can be used to reconstruct WSI extent.

3.4. *N. pachyderma* $\delta^{18}O_c$ as Tracer for Winter Water

We propose that the planktonic foraminiferal species *N. pachyderma* can be used to estimate sub-surface $\delta^{18}O_c$ in the geologic past. *N. pachyderma* lives year-round in Antarctic surface waters, including austral winter when it is found near the sea ice edge and in sea ice itself (Dieckmann et al., 1991; Hendry et al., 2009; Lipps & Krebs, 1974; Spindler & Dieckmann, 1986). Reported densities of *N. pachyderma* routinely exceed 20,000 individuals per cubic meter of melted sea ice, including live and dead individuals (Lipps & Krebs, 1974; Spindler & Dieckmann, 1986). *N. pachyderma* are apparently incorporated into sea ice during ice growth and survive in brine channels by feeding on abundant diatoms (Spindler & Dieckmann, 1986). Because brine formation has little influence on $\delta^{18}O_{sw}$ (Tan & Strain, 1996), the $\delta^{18}O_c$ of *N. pachyderma* will primarily reflect temperature.

Previous studies imply that the $\delta^{18}O_c$ of *N. pachyderma* is offset from its expected equilibrium $\delta^{18}O_c$. *N. pachyderma* has been shown to have $\delta^{18}O_c$ values ranging from ~1‰ lower than equilibrium (Bauch et al., 1997; Mortyn & Charles, 2003; Norris et al., 1998) to ~0.5‰ higher than equilibrium (Kohfeld et al., 1996; Matsumoto et al., 2001). In the studies, predicted $\delta^{18}O_c$ values were based on the O'Neil et al. (1969) temperature

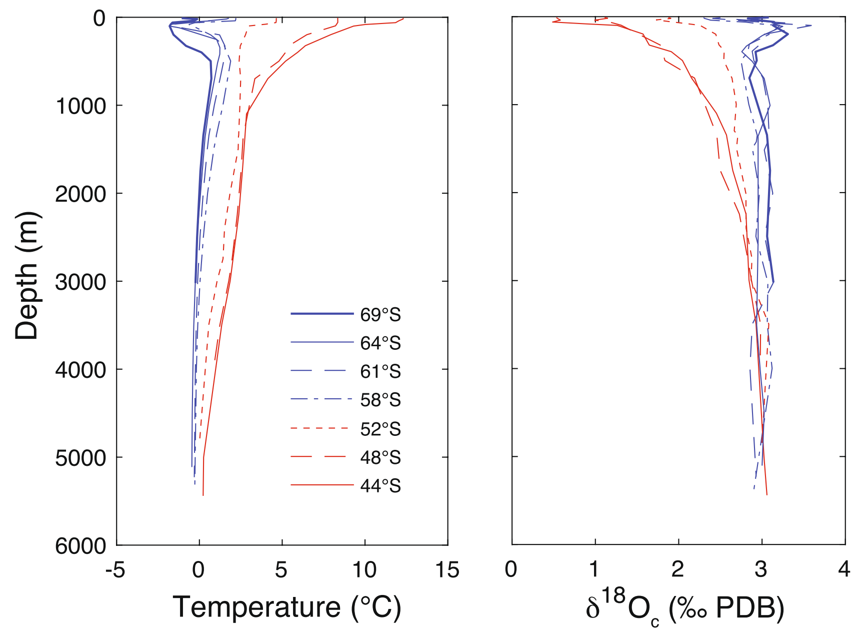

Figure 6. Vertical profiles of in situ temperature (left panel) and predicted equilibrium $\delta^{18}O_c$ (right panel) from ∼30°E (Archambeau et al., 1998). The $\delta^{18}O_c$ estimates are based on the quadratic equation for *Cibicidoides* spp. (Marchitto et al., 2014). Hydrographic data represent austral summer conditions (March 1993).

calibration. The more recent calibration of Kim and O'Neil (1997) yields equilibrium $\delta^{18}O_c$ estimates that are in better agreement with foraminiferal results, however, particularly at the cold end of the temperature spectrum (Marchitto et al., 2014). For example, when the predicted $\delta^{18}O_c$ for the Bauch et al. (1997) data are determined using the Kim and O'Neil (1997) calibration, the average offset with *N. pachyderma* $\delta^{18}O_c$ decreases to ∼0.1‰. Similarly, Livsey et al. (2020) found that *N. pachyderma* $\delta^{18}O_c$ in the hydrographically complex Fram Strait have an average offset from equilibrium values of 0.3 ± 0.8‰ (using the Kim and O'Neil (1997) equation). Calcification temperature is another key consideration when calculating $\delta^{18}O_c$. In the case of the core top studies (Kohfeld et al., 1996; Matsumoto et al., 2001), it was assumed that *N. pachyderma* calcifies in equilibrium with summer sea surface temperatures. As a result, the predicted $\delta^{18}O_c$ values skewed toward the light end of the spectrum, making *N. pachyderma* $\delta^{18}O_c$ isotopically heavy by comparison.

Here, we estimate equilibrium $\delta^{18}O_c$ values using the non-linear temperature calibration from Marchitto et al. (2014):

$$\delta^{18}O_c\left(PDB\right) - \delta^{18}O_{sw}\left(SMOW\right) + 0.27 = -0.245t + 0.0011t^2 + 3.58$$

where t is in situ temperature (°C), $\delta^{18}O_c$ is expressed relative to PDB (‰), and $\delta^{18}O_{sw}$ is expressed relative to SMOW (‰). Following convention, we add 0.27‰ to $\delta^{18}O_{sw}$ to convert from the SMOW to PDB scale (Hut, 1987). The above equation is based on more than 100 benthic foraminiferal $\delta^{18}O_c$-$\delta^{18}O_{sw}$ pairs spanning −1°C to 20°C. It also yields $\delta^{18}O_c$ estimates indistinguishable from the Kim and O'Neil (1997) calibration (Marchitto et al., 2014). The resulting $\delta^{18}O_c$ values are therefore more positive than those calculated using older equations (O'Neil et al., 1969; Marchitto et al., 2014; Shackleton, 1974). The source of our temperature and $\delta^{18}O_{sw}$ data are the NASA-Goddard seawater $\delta^{18}O$ database (https://data.giss.nasa.gov/o18data/), which we use because the $\delta^{18}O_{sw}$ data are based on in situ observations. In situ observations are preferable to estimates based on regional $\delta^{18}O_{sw}$-salinity relationships because $\delta^{18}O_{sw}$ and salinity can become decoupled in areas of melting of sea ice (Bauch et al., 1997; Norris et al., 1998).

Hydrographic data from the study area are shown in Figure 7, including, from left to right, panels depicting temperature, salinity, $\delta^{18}O_{sw}$, and the predicted $\delta^{18}O_c$ of calcite. The top row of panels displays austral summer conditions (JFM), while the bottom row is for austral winter (ASO). During winter, the predicted

10.1029/2020PA004095

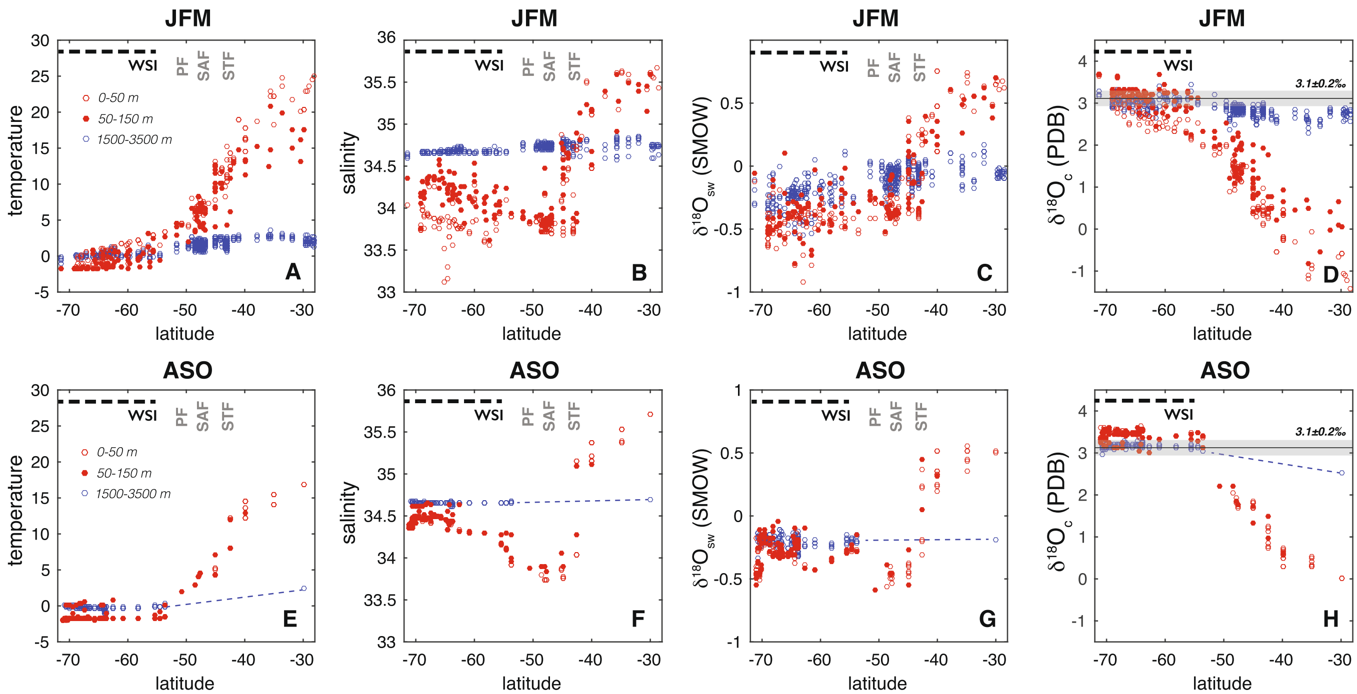

Figure 7. Latitudinal transects of in situ temperature, salinity, $\delta^{18}O_{sw}$ and calculated equilibrium $\delta^{18}O_c$ for the Atlantic and Indian sectors of the Southern Ocean (50°W to 60°E) for austral summer (JFM; top row) and winter (ASO; bottom row). Data are partitioned into surface (0–50 m; open red circles), sub-surface (50–150 m; solid red circles), and deep ocean (1,500–3,500 m; blue circles). Also shown are the climatological extent of winter sea ice (WSI) at 0°E (horizontal dashed lines) (https://nsidc.org) and the approximate position of the Polar Front (PF), Sub-Antarctic Front (SAF) and Subtropical Front (STF) (vertical gray text) (Orsi et al., 1995). Winter sea ice extent corresponds to the zone where JFM sub-surface temperatures are colder than deep ocean temperatures (a) and where the calculated JFM sub-surface $\delta^{18}O_c$ is greater than deep ocean $\delta^{18}O_c$ (d). Also shown is the equilibrium $\delta^{18}O_c$ for the −0.5°C WW isotherm (3.1 ± 0.2‰; thin horizontal line and shaded bar). The estimated in $\delta^{18}O_c$ uncertainty reflects the two-sigma range in $\delta^{18}O_{sw}$ (c and g). Hydrographic data are from the NASA-GISS seawater $\delta^{18}O$ database (https://data.giss.nasa.gov/o18data/).

$\delta^{18}O_c$ for surface (0–50 m) and subsurface (50–150 m) waters reaches a maximum of 3.5‰ in the seasonal sea ice zone (Figure 7h), a value that is set by the freezing point of seawater (Figure 7e). During summer, surface layer $\delta^{18}O_c$ averages ~2.5‰ in the seasonal sea ice zone, compared to ~3.0‰ in the sub-surface layer (Figure 7d), where the higher $\delta^{18}O_c$ values are due to the presence of WW (Figure 7a). The $\delta^{18}O_c$ difference between the layers (~0.5‰) is similar to the offset between *N. pachyderma* and equilibrium $\delta^{18}O_c$ observed in core top studies, implying the predicted $\delta^{18}O_c$ in these studies was too low due to the use of warmer surface calcification temperatures. If *N. pachyderma* instead calcifies in colder sub-surface WW, the apparent offset in predicted and observed $\delta^{18}O_c$ largely disappears.

Plankton tow results from polar regions indicate that the depth habitat of *N. pachyderma* overlaps with the depth range of WW. In the Southern Ocean, the results from three different plankton tow studies show that *N. pachyderma* resides in the upper 200 m of the water column (Kohfeld et al., 2000; Mortyn & Charles, 2003; Meilland et al., 2018). Similarly, a compilation of 104 plankton tow studies from the Arctic and North Atlantic indicates that the abundance weighted habitat depth for *N. pachyderma* is 100 ± 41 m (1σ) (Greco et al., 2019). It is important to note, however, that the Arctic and Antarctic are inhabited by distinct genotypes of *N. pachyderma* (Darling et al., 2004, 2007). Whether the observed genetic differences translate into unique depth habitats remain unknown. But the available data indicate that *N. pachyderma* primarily resides in the upper 150 m of the water column, intersecting the depth range of WW.

Additionally, sediment trap results suggest = *N. pachyderma* calcifies in equilibrium with WW. At Maud Rise, the $\delta^{18}O_c$ of *N. pachyderma* in the >250 μm size fraction exceeds 3.2‰ throughout the year, with the heaviest $\delta^{18}O_c$ values occurring in January and February (Donner & Wefer, 1994). As discussed above, planktonic $\delta^{18}O_c$ results >3‰ are consistent with calcification in WW (Figure 7d). The highest fluxes of *N. pachyderma* at Maud Rise occur during January through March, when WW is located at ~50–100 m water depth (Figure S1). Trap results from the West Antarctic Peninsula show a similar pattern, with the heaviest *N.*

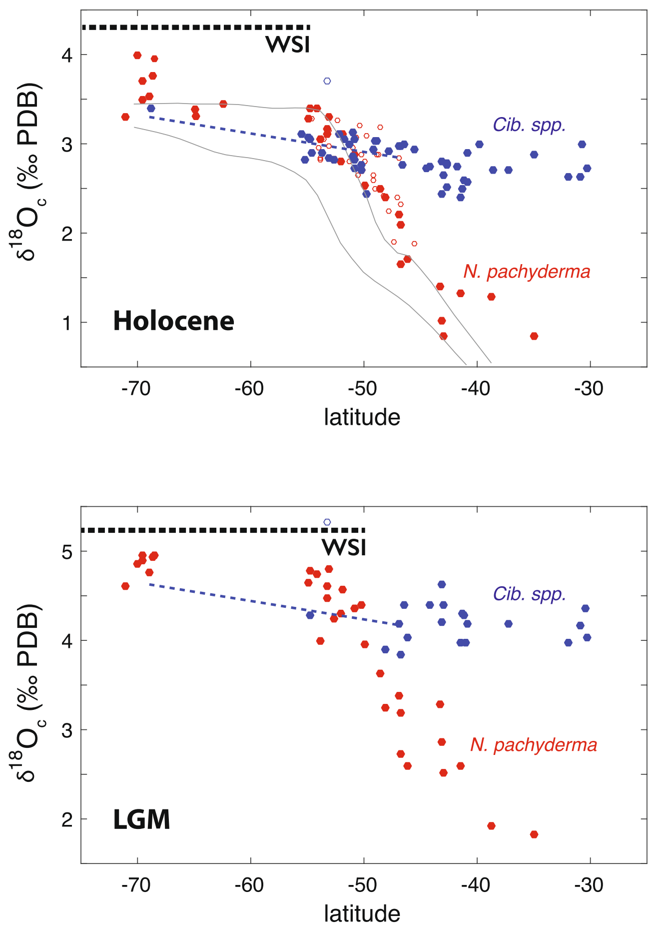

Figure 8. Atlantic sector transects of planktonic and benthic $\delta^{18}O_c$. (Top) Holocene, including *N. pachyderma* (red) and *Cibicidoides* spp. (blue). Also noted is the modern winter sea ice extent (horizontal dashed line) (Figure 2), the Gaussian-smoothed equilibrium surface $\delta^{18}O_c$ for winter (upper gray line) and summer (lower gray line), and the deep ocean $\delta^{18}O_c$ trend from Figure 7 (blue-dashed line). Open red symbols denote *N. pachyderma* results from the tops of cores that lack chronostratigraphic information. (Bottom) Same as top panel but for the LGM, including winter sea ice extent based on diatom assemblages (horizontal dashed line) (Gersonde et al., 2003). The trend in benthic $\delta^{18}O_c$ from 50°S to 70°S is shown for reference (dashed blue line; see text for details). Benthic data for ODP 1094 at 53°S are shown as light blue symbols (Hasenfratz et al., 2019). For reasons that are unclear, the Holocene benthic $\delta^{18}O_c$ reported for this core averages 3.7‰, which is 0.7‰ higher than both the expected equilibrium value and the mean benthic $\delta^{18}O_c$ based on 10 nearby cores. The estimated mean LGM benthic $\delta^{18}O_c$ for ODP 1094 is 5.3‰, or ~1‰ higher than nearby results. All of the data depicted in Figure 8 are summarized in Table S1.

pachyderma $\delta^{18}O_c$ coinciding with intervals of maximum shell flux from December through February (Mikis et al., 2019). These isotopically heavy individuals have completed their full life cycle, as indicated by their large (>250 μm) spherical tests and clear evidence for secondary encrustation (Mikis et al., 2019; Kohfeld et al., 1996). The heavier $\delta^{18}O_c$ of the secondary calcite reflects calcification deeper in the water column under cooler ambient conditions (Kozdon et al., 2009). Because the mass of individual *N. pachyderma* shells is dominated by their crust (Kohfeld et al., 1996), so too is their $\delta^{18}O_c$ signature (Kozdon et al., 2009). At the West Antarctic Peninsula trap site, the $\delta^{18}O_c$ of large individuals (>3‰) is consistent with addition of secondary crust in equilibrium with WW at ~50–100 m, where temperatures range from 0°C to −1°C (Mikis et al., 2019). Becuase the flux of large individuals during summertime dominates the annual shell flux, the oxygen isotopic signature of mature, encrusted *N. pachyderma* in seafloor samples should reflect the $\delta^{18}O_c$ of WW.

4. Results and Discussion

Do core top data support our assertion that *N. pachyderma* $\delta^{18}O_c$ can be used to map WW and therefore sea ice extent? To address this question, we adopt the approach of Matsumoto et al. (2001), who used the intersection of planktonic and benthic $\delta^{18}O_c$ trends in the Southern Ocean to infer the position of the Polar Front (Figure 8). Here, we supplement their Atlantic sector data using records published since 2001 (Table S1). During the Holocene, *N. pachyderma* $\delta^{18}O_c$ values are persistently high (>3.3‰) from 70°S to 55°S and then decrease moving northward (Figure 8). The results are similar to the estimated equilibrium $\delta^{18}O_c$ for wintertime conditions in the upper 150 m, which reflect near freezing temperatures in the seasonal sea ice zone and progressively warmer conditions in the sub-Antarctic and sub-tropical Atlantic. In contrast to the planktonic results, benthic $\delta^{18}O_c$ decreases by only ~0.4‰ from 70°S to 30°S, due to the relatively homogenous temperature and $\delta^{18}O_{sw}$ characteristics of CDW (Figure 7). Higher benthic $\delta^{18}O_c$ values south of 45°S are due to geostrophic flow of the Antarctic Circumpolar Current and the upward tilting of isopycnals toward Antarctica (Figure 1). The area where *N. pachyderma* $\delta^{18}O_c$ exceeds benthic $\delta^{18}O_c$ (70°S to 55°S) coincides with the zone of maximum winter sea ice extent (Figure 8). Thus, initial core top results from the Atlantic sector suggest $\Delta\delta^{18}O_c$ can be used to map the sea ice edge.

The spatial trends in planktonic and benthic $\delta^{18}O_c$ during the LGM are broadly consistent with those during the Holocene. *N. pachyderma* $\delta^{18}O_c$ is persistently high from 70°S to ~53°S, with monotonically decreasing values north of 50°S (Figure 8). The benthic $\delta^{18}O_c$ data are sparse by comparison but show little variability from 55°S to 30°S. The core site at 55°S has a mean planktonic $\delta^{18}O_c$ that is 0.5‰ higher than the mean benthic $\delta^{18}O_c$ in the same core, which is consistent with winter sea ice reaching this location. But overall the LGM data are too limited to make any conclusive statements about sea ice extent. We can, however, estimate the likely trend in LGM benthic $\delta^{18}O_c$ south of the PF using modern and Holocene constraints. Today, the equilibrium $\delta^{18}O_c$ of CDW decreases by 0.4‰ from 70°S to 45°S (Figure 7), similar to the late Holocene trend in benthic $\delta^{18}O_c$ (Figure 8). Assuming that the latitudinal gradient of $\delta^{18}O_c$ surfaces was similar during the LGM, we superimpose the late Holocene $\delta^{18}O_c$ gradient on the LGM data after adding 1.4‰, which is the mean LGM-Holocene difference in benthic $\delta^{18}O_c$ from 48°S to 30°S, where there is reasonably high LGM coverage. Most of the planktonic data from 70°S to 52°S plot above the resulting trendline (dashed blue), implying this region was covered by sea ice at least part of the year. By comparison, diatom-based estimates near 0°E suggest that the WSI edge was located at ~50°S (Crosta et al., 1998; Gersonde et al., 2003).

4.1. Planktonic $\delta^{18}O_c$ Plateau

In the preceding sections, we outlined a method for estimating WSI extent using paired analyses of planktonic and benthic foraminifera. However, planktonic $\delta^{18}O_c$ alone may be an effective proxy for sea ice extent. Our analysis of modern hydrographic data indicates that the summertime position of the −0.5°C and 0°C WW isotherms track the WSI edge, with a latitudinal uncertainty of ~ ±1° (Figure 3). In the depth range of WW, the mean $\delta^{18}O_{sw}$ south of the PF is −0.35 ± 0.2‰ (2σ) (Figure 7). The resulting equilibrium $\delta^{18}O_c$ associated with −0.5°C WW is therefore 3.1 ± 0.2‰. For the 0°C isotherm, it is nearly the same, 3.0 ± 0.2‰. Given the spatial relationship between WW isotherms and WSI extent, equilibrium $\delta^{18}O_c$ values greater than 3.3‰ should generally occur south of the WSI edge, while $\delta^{18}O_c$ values less than 3.3‰ should occur north of it. As shown in Figure 7d, this is indeed the case; predicted equilibrium $\delta^{18}O_c$ values at or above the 3.3‰ threshold occur entirely in the seasonal sea ice zone. For the late Holocene, *N. pachyderma* $\delta^{18}O_c$ data exceed 3.3‰ south of ~54°S (Figure 8). The climatological winter sea ice edge in this region (20°W to 20°E) occurs at 55°S (Figure 2). Thus, *N. pachyderma* $\delta^{18}O_c$ results on their own yield an estimate of winter sea ice extent consistent with modern observations.

The Holocene *N. pachyderma* results are characterized by a plateau of $\delta^{18}O_c$ values at or above ~3.3‰ (Figure 8). There is a slope in the $\delta^{18}O_c$ plateau, however, which is likely due to individual foraminifera calcifying in water warmer than 0°C. Given the small mass of individual *N. pachyderma* shells, multiple shells are typically required to yield adequate CO_2 for stable isotope analysis. Thus, as one moves toward warmer latitudes, the likelihood of incorporating individuals that calcified in warmer WW should increase, resulting in a lower mean $\delta^{18}O_c$. Future studies can address this potential issue by analyzing individual *N. pachyderma* specimens (Metcalfe et al., 2019; Mikis et al., 2019).

4.2. Caveats

While our preliminary results for the Holocene are encouraging, there are several caveats to consider. First, our approach is necessarily limited to those areas of the Southern Ocean where foraminifera are preserved, such mid-ocean ridges and plateaus. Second, the planktonic-benthic $\delta^{18}O_c$ signal associated with the seasonal sea ice zone is comparable to observed interlaboratory $\delta^{18}O_c$ offsets of ~0.3‰ (Hodell et al., 2003; Ostermann & Curry, 2000). Future efforts to constrain sea ice extent should therefore be based on $\delta^{18}O_c$ data from a single laboratory or on carefully intercalibrated results from different labs. This will be particularly important for inferring the inflection point in planktonic $\delta^{18}O_c$ near the WSI edge. Third, the depth range of *N. pachyderma* in the seasonal sea ice zone is poorly constrained. While it appears that mature *N. pachyderma* calcify in WW, an improved understanding of their depth habitat will require plankton tow studies in the seasonal sea ice zone during austral spring/summer when shells fluxes are at their annual maximum. Finally, warm WW isotherms (>0°C) can exist well north of the sea ice edge, which complicates the use of foraminiferal $\delta^{18}O_c$ as a sea ice proxy. Efforts to constrain sea ice extent will therefore need to carefully assess the difference between co-located planktonic and benthic $\delta^{18}O_c$ results, the spatial pattern in planktonic $\delta^{18}O_c$ data, and the absolute value of $\delta^{18}O_c$ to determine relative movement of WW isotherms. Given these caveats, we recommend that the $\delta^{18}O_c$ method, like any proxy, be used as part of a multi-proxy strategy to reconstruct sea ice in the geologic past.

5. Conclusions

We present a new method to estimate winter sea ice extent that is based on the unique vertical temperature profile in the seasonal sea ice zone of the Southern Ocean. Sea ice formation and brine rejection durting austral winter create a deep mixed layer characterized by near freezing temperatures. Enhanced solar heating and ice melt during austral summer creates a warm and fresh surface layer that caps the winter mixed layer, creating a cold sub-surface remnant known as winter water (WW). The superposition of cold WW over relatively warm Circumpolar Deep Water creates an inverted temperature profile in the seasonal sea ice zone. The unique temperature conditions yield an equilibrium $\delta^{18}O_c$ profile where surface mixed layer $\delta^{18}O_c$ is greater than deeper in the water column. As a result, the difference between planktonic and benthic foraminiferal $\delta^{18}O$ ($\Delta\delta^{18}O$) can be used as a proxy for winter water and sea ice extent, where areas with positive $\Delta\delta^{18}O$ are conducive to sea ice formation, while areas with negative $\Delta\delta^{18}O_c$ values are too warm to support ice growth.

To determine the spatial relationship between WW and WSI, we mapped WW isotherms using WOCE sections and gridded data products from the Southern Ocean. Our findings suggest that the −0.5°C WW isotherm, which equates to an equilibrium $\delta^{18}O_c$ of 3.1 ± 0.2‰, most closely aligns with the winter sea ice edge. Sub-surface equilibrium $\delta^{18}O_c$ values >3.3‰ only occur in the seasonal sea ice zone and they are greater than co-located deep ocean equilibrium $\delta^{18}O_c$ results. Thus, the difference between surface and deep ocean $\delta^{18}O_c$ can be used as a proxy for sea ice extent.

To evaluate the $\delta^{18}O_c$ method, we present a compilation of planktonic and benthic $\delta^{18}O_c$ from the Atlantic sector of the Southern Ocean. We find that: (a) the $\delta^{18}O_c$ of *N. pachyderma* is consistent with calcification in cold sub-surface WW, and (b) that $\delta^{18}O_c$ values >3.3‰ occur only in the seasonal sea ice zone. Furthermore, we show that the difference between planktonic and benthic $\delta^{18}O_c$ ($\Delta\delta^{18}O_c$) is positive as far north as 54°S, similar to the latitude of the winter sea ice edge inferred from satellite observations (~55°S). Preliminary results for the LGM are inconclusive, mainly due to an absence of benthic data. While the initial Holocene results are encouraging, the $\delta^{18}O_c$ method requires further testing using data from other sectors of the Southern Ocean where foraminifera are preserved and cross-validation with existing sea ice reconstruction techniques. The depth range in which *N. pachyderma* calcifies also needs to be verified using plankton tow results from the seasonal sea ice zone during austral spring and summer, when shell fluxes are highest. Analyses of individual *N. pachyderma* shells will also be helpful to determine the maximum $\delta^{18}O_c$ at a given latitude, which will allow for improved visualization of the planktonic $\delta^{18}O_c$ plateau associated with the seasonal sea ice zone. Finally, we suggest that model simulations can be used to improve our understanding of the spatial relationship between WW and WSI extent in the modern Southern Ocean and to provide constraints on the expected LGM $\delta^{18}O_c$ signal associated with northward expansion of the WSI edge.

Data Availability Statement

The ARGO data depicted in Figure S2 were collected and made freely available by the International Argo Program and the national programs that contribute to it (http://www.argo.ucsd.edu, http://argo.jcommops.org). The Argo Program is part of the Global Ocean Observing System. The stable isotope data in Figure 8 are summarized in Table S1 and are available on the NOAA Paleoclimatology Data website (http://www.ncdc.noaa.gov/data-access/paleoclimatology-data).

Acknowledgments
We would like to thank three anonymous reviewers for their constructive suggestions that markedly improved the initial submission. This work has also benefitted from discussions with Steve Rintoul, Liz Sikes, and Jess Adkins. In particular, we would like to thank Will Hobbs for generously sharing his knowledge of Southern Ocean sea ice and the processes that govern its modern distribution.

References

Abernathey, R. P., Cerovecki, I., Holland, P. R., Newsom, E., Mazloff, M., & Talley, L. D. (2016). Water-mass transformation by sea ice in the upper branch of the Southern Ocean overturning. *Nature Geoscience*, *9*(8), 596–601. https://doi.org/10.1038/ngeo2749

Abram, N. J., Wolff, E. W., & Curran, M. A. J. (2013). A review of sea ice proxy information from polar ice cores. *Quaternary Science Reviews*, *79*, 168–183. https://doi.org/10.1016/j.quascirev.2013.01.011

Adkins, J. F. (2013). The role of deep ocean circulation in setting glacial climates. *Paleoceanography*, *28*(3), 539–561. https://doi.org/10.1002/palo.20046

Adkins, J. F., McIntyre, K., & Schrag, D. P. (2002). The salinity, temperature, and delta 18O of the glacial deep ocean. *Science*, *298*(5599), 1769–1773. https://doi.org/10.1126/science.1076252

Allen, C. S., Pike, J., & Pudsey, C. J. (2011). Last glacial-interglacial sea-ice cover in the SW Atlantic and its potential role in global deglaciation. *Quaternary Science Reviews*, *30*, 2446–2458. https://doi.org/10.1016/j.quascirev.2011.04.002

Archambeau, A.-S., Pierre, C., Poisson, A., & Schauer, B. (1998). Distributions of oxygen and carbon stable isotopes and CFC-12 in the water masses of the Southern Ocean at 30°E from South Africa to Antarctica: Results of the CIVA1 cruise. *Journal of Marine Systems*, *17*(1–4), 25–38. https://doi.org/10.1016/s0924-7963(98)00027-x

Bauch, D., Carstens, J., & Wefer, G. (1997). Oxygen isotope composition of living *Neogloboquadrina pachyderma* (sin.) in the Arctic Ocean. *Earth and Planetary Science Letters*, *146*(1–2), 47–58. https://doi.org/10.1016/s0012-821x(96)00211-7

Belkin, I. M., & Gordon, A. L. (1996). Southern Ocean fronts from the Greenwich meridian to Tasmania. *Journal of Geophysical Research*, *101*(C2), 3675–3696. https://doi.org/10.1029/95jc02750

Belt, S. T. (2018). Source-specific biomarkers as proxies for Arctic and Antarctic sea ice. *Organic Geochemistry*, *125*, 277–298. https://doi.org/10.1016/j.orggeochem.2018.10.002

Belt, S. T., Smik, L., Brown, T. A., Kim, J. H., Rowland, S. J., Allen, C. S., et al. (2016). Source identification and distribution reveals the potential of the geochemical Antarctic sea ice proxy IPSO25. *Nature Communications*, *7*(1), 12655. https://doi.org/10.1038/ncomms12655

Benz, V., Esper, O., Gersonde, R., Lamy, F., & Tiedemann, R. (2016). Last glacial maximum sea surface temperature and sea-ice extent in the Pacific sector of the Southern Ocean. *Quaternary Science Reviews*, *146*(2016), 216–237. https://doi.org/10.1016/j.quascirev.2016.06.006

Burckle, L. H. (1983). Diatom dissolution patterns in sediments of the Southern ocean. *Geological Society of America Journal*, *15*, 536–537.

Burckle, L. H., & Cirilli, J. (1987). Origin of Diatom Ooze Belt in the Southern Ocean: Implications for late quaternary paleoceanography. *Micropaleontology*, *33*(1), 82–86. https://doi.org/10.2307/1485529

Burckle, L. H., & Mortlock, R. (1998). Sea-ice extent in the Southern Ocean during the Last Glacial Maximum: Another approach to the problem. *Annals of Glaciology*, *27*, 302–304. https://doi.org/10.3189/1998aog27-1-302-304

Burckle, L. H., Robinson, D., & Cooke, D. (1982). Reappraisal of sea-ice distribution in Atlantic and Pacific sectors of the Southern Ocean at 18,000 yr BP. *Nature*, *299*(5882), 435–437. https://doi.org/10.1038/299435a0

CLIMAP Project Members. (1976). The surface of the ice age Earth. *Science*, *191*, 1131–1137.

Collins, L. G., Allen, C. S., Pike, J., Hodgson, D. A., Weckström, K., & Massé, G. (2013). Evaluating highly branched isoprenoid (HBI) biomarkers as a novel Antarctic sea-ice proxy in deep ocean glacial age sediments. *Quaternary Science Reviews*, *79*, 87–98. https://doi.org/10.1016/j.quascirev.2013.02.004

Collins, L. G., Pike, J., Allen, C. S., & Hodgson, D. A. (2012). High-resolution reconstruction of southwest Atlantic sea-ice and its role in the carbon cycle during marine isotope stages 3 and 2. *Paleoceanography*, *27*. https://doi.org/10.1029/2011pa002264

Crosta, X., Pichon, J.-J., & Burckle, L. H. (1998). Application of modern analog technique to marine Antarctic diatoms: Reconstruction of maximum sea-ice extent at the last glacial maximum. *Paleoceanography*, *13*(3), 284–297. https://doi.org/10.1029/98pa00339

Crosta, X., Sturm, A., Armand, L., & Pichon, J.-J. (2004). Late Quaternary sea ice history in the Indian sector of the Southern Ocean as recorded by diatom assemblages. *Marine Micropaleontology*, *50*, 209–223. https://doi.org/10.1016/s0377-8398(03)00072-0

Cunningham, S. A., Alderson, S. G., King, B. A., & Brandon, M. A. (2003). Transport and variability of the Antarctic Circumpolar Current in Drake Passage. *Journal of Geophysical Research*, *108*(5). https://doi.org/10.1029/2001jc001147

Darling, K. F., Kucera, M., Pudsey, C. J., & Wade, C. M. (2004). Molecular evidence links cryptic diversification in polar planktonic protists to Quaternary climate dynamics. *Proceedings of the National Academy of Sciences*, *101*(20), 7657–7662. https://doi.org/10.1073/pnas.0402401101

Darling, K. F., Kucera, M., & Wade, C. M. (2007). Global molecular phylogeography reveals persistent Arctic circumpolar isolation in a marine planktonic protist. *Proceedings of the National Academy of Sciences*, *104*(12), 5002–5007. https://doi.org/10.1073/pnas.0700520104

De Boer, A. M., & Hogg, A. M. (2014). Control of the glacial carbon budget by topographically induced mixing. *Geophysical Research Letters*, *41*(12), 4277–4284. https://doi.org/10.1002/2014gl059963

DeFelice, D. R. (1979). *Surface Lithofacies, Biofacies, and diatom Diversity patterns as models for Delineation of climatic change in the Southeast Atlantic ocean*. (Ph.D.). Florida State University.

Dieckmann, G. S., Spindler, M., Lange, M. A., Ackley, S. F., & Eicken, H. (1991). Antarctic sea ice; a habitat for the foraminifer Neogloboquadrina pachyderma. *Journal of Foraminiferal Research*, *21*(2), 182–189. https://doi.org/10.2113/gsjfr.21.2.182

Donner, B., & Wefer, G. (1994). Flux and stable isotope composition of Neogloboquadrina pachyderma and other planktonic foraminifers in the Southern Ocean (Atlantic sector). *Deep Sea Research Part I: Oceanographic Research Papers*, *41*(11–12), 1733–1743. https://doi.org/10.1016/0967-0637(94)90070-1

Eggleston, S., & Galbraith, E. D. (2018). The devil's in the disequilibrium: Multi-component analysis of dissolved carbon and oxygen changes under a broad range of forcings in a general circulation model. *Biogeosciences*, *15*(12), 3761–3777. https://doi.org/10.5194/bg-15-3761-2018

Esper, O., & Gersonde, R. (2014). New tools for the reconstruction of Pleistocene Antarctic sea ice. *Palaeogeography, Palaeoclimatology, Palaeoecology*, *399*, 260–283. https://doi.org/10.1016/j.palaeo.2014.01.019

Esper, O., Gersonde, R., & Kadagies, N. (2010). Diatom distribution in southeastern Pacific surface sediments and their relationship to modern environmental variables. *Palaeogeography, Palaeoclimatology, Palaeoecology*, *287*(1), 1–27. https://doi.org/10.1016/j.palaeo.2009.12.006

Ferrari, R., Jansen, M. F., Adkins, J. F., Burke, A., Stewart, A. L., & Thompson, A. F. (2014). Antarctic sea ice control on ocean circulation in present and glacial climates. *Proceedings of the National Academy of Sciences*, *111*(24), 8753–8758. https://doi.org/10.1073/pnas.1323922111

Ferry, A. J., Prvan, T., Jersky, B., Crosta, X., & Armand, L. K. (2015). Statistical modeling of Southern Ocean marine diatom proxy and winter sea ice data: Model comparison and developments. *Progress in Oceanography*, *131*, 100–112. https://doi.org/10.1016/j.pocean.2014.12.001

Fraser, C. I., Nikula, R., Spencer, H. G., & Waters, J. M. (2009). Kelp genes reveal effects of subantarctic sea ice during the Last Glacial Maximum. *Proceedings of the National Academy of Sciences*, *106*(9), 3249–3253. https://doi.org/10.1073/pnas.0810635106

Galbraith, E., & de Lavergne, C. (2019). Response of a comprehensive climate model to a broad range of external forcings: Relevance for deep ocean ventilation and the development of late Cenozoic ice ages. *Climate Dynamics*, *52*(1–2), 653–679. https://doi.org/10.1007/s00382-018-4157-8

Galbraith, E. D., & Skinner, L. C. (2020). The Biological Pump during the Last Glacial Maximum. *Annual Review of Marine Science*, *12*, 559–586. https://doi.org/10.1146/annurev-marine-010419-010906

Gersonde, R., Abelmann, A., Brathauer, U., Becquey, S., Bianchi, C., Cortese, G., et al. (2003). Last glacial sea surface temperatures and sea-ice extent in the Southern Ocean (Atlantic-Indian sector): A multiproxy approach. *Paleoceanography*, *18*(3), 6–18. https://doi.org/10.1029/2002pa000809

Gersonde, R., Crosta, X., Abelmann, A., & Armand, L. (2005). Sea-surface temperature and sea ice distribution of the Southern Ocean at the EPILOG Last Glacial Maximum - A circum-Antarctic view based on siliceous microfossil records. *Quaternary Science Reviews*, *24*(7–9), 869–896. https://doi.org/10.1016/j.quascirev.2004.07.015

Gersonde, R., & Zielinski, U. (2000). The reconstruction of late Quaternary Antarctic sea-ice distribution-the use of diatoms as a proxy for sea-ice. *Palaeogeography, Palaeoclimatology, Palaeoecology*, *162*(3–4), 263–286. https://doi.org/10.1016/s0031-0182(00)00131-0

Gordon, A. L., & Huber, B. A. (1984). Thermohaline stratification below the southern ocean sea ice. *Journal of Geophysical Research*, *89*(C1), 641–648. https://doi.org/10.1029/jc089ic01p00641

Gupta, M., Folllows, M. J., & Lauderdale, J. M. (2020). The effect of Antarctic sea ice on Southern Ocean carbon outgassing: Capping versus light attenuation. *Global Biogeochemical Cycles*, 34, 1–50.

Hasenfratz, A. P., Jaccard, S. L., Martínez-García, A., Sigman, D. M., Hodell, D. A., Vance, D., et al. (2019). The residence time of Southern Ocean surface waters and the 100,000-year ice age cycle. *Science*, *363*(6431), 1080–1084. https://doi.org/10.1126/science.aat7067

Haumann, F. A., Gruber, N., Münnich, M., Frenger, I., & Kern, S. (2016). Sea-ice transport driving Southern Ocean salinity and its recent trends. *Nature*, *537*(7618), 89–92. https://doi.org/10.1038/nature19101

Hays, J. D., Lozano, J. A., Shackleton, N., & Irving, G. (1976). Reconstruction of the Atlantic and western Indian Ocean sectors of the 18,000 B.P. Antarctic Ocean Memoir of the Geological Society of America *145*, 337–372. https://doi.org/10.1130/mem145-p337

Hendry, K., Rickaby, R., Meredith, M., & Elderfield, H. (2009). Controls on stable isotope and trace metal uptake in Neogloboquadrina pachyderma (sinistral) from an Antarctic sea-ice environment. *Earth and Planetary Science Letters*, *278*(1–2), 67–77. https://doi.org/10.1016/j.epsl.2008.11.026

Hobbs, W. R., Massom, R., Stammerjohn, S., Reid, P., Williams, G., & Meier, W. (2016). A review of recent changes in Southern Ocean sea ice, their drivers and forcings. *Global and Planetary Change*, *143*, 228–250. https://doi.org/10.1016/j.gloplacha.2016.06.008

Hodell, D. A., Charles, C. D., Curtis, J. H., Graham Mortyn, P., Ninnemann, U. S., & Venz, K. A. (2003). Data report: Oxygen isotope stratigraphy of leg 177 Sites 1088, 1089, 1090, 1093, 1094. In R. Gersonde, D. A. Hodell, & P. Blum, (Eds.), *Proceedings of the ocean Drilling program, Scientific results* (Vol. *177*).

Hut, G. (1987). *Consultants' group meeting on stable isotope reference samples for geochemical and hydrological investigations*.

Jansen, M. F., & Nadeau, L.-P. (2016). The effect of Southern Ocean surface buoyancy loss on the deep-ocean circulation and stratification. *Journal of Physical Oceanography*, *46*(11), 3455–3470. https://doi.org/10.1175/jpo-d-16-0084.1

Khatiwala, S., Schmittner, A., & Muglia, J. (2019). Air-sea disequilibrium enhances ocean carbon storage during glacial periods. *Science Advances*, *5*(6). https://doi.org/10.1126/sciadv.aaw4981

Kim, S.-T., & O'Neil, J. R. (1997). Equilibrium and nonequilibrium oxygen isotope effects in synthetic carbonates. *Geochimica et Cosmochimica Acta*, *61*(16), 3461–3475. https://doi.org/10.1016/s0016-7037(97)00169-5

Kohfeld, K. E., Anderson, R. F., & Lynch-Stieglitz, J. (2000). Carbon isotopic disequilibrium in polar planktonic foraminifera and its impact on modern and Last Glacial Maximum reconstructions. *Paleoceanography*, *15*(1), 53–64. https://doi.org/10.1029/1999pa900049

Kohfeld, K. E., Fairbanks, R. G., Smith, S. L., & Walsh, I. D. (1996). Neogloboquadrina pachyderma (sinistral coiling) as paleoceanographic tracers in polar oceans: Evidence from northeast water polynya plankton tows, sediment traps, and surface sediments. *Paleoceanography*, *11*(6), 679–699. https://doi.org/10.1029/96pa02617

Kozdon, R., Ushikubo, T., Kita, N. T., Spicuzza, M., & Valley, J. W. (2009). Intratest oxygen isotope variability in the planktonic foraminifer *N. pachyderma*: Real vs. apparent vital effects by ion microprobe. *Chemical Geology*, *258*(3–4), 327–337. https://doi.org/10.1016/j.chemgeo.2008.10.032

Kucera, M., Rosell-Melé, A., Schneider, R., Waelbroeck, C., & Weinelt, M. (2005). Multiproxy approach for the reconstruction of the glacial ocean surface (MARGO). *Quaternary Science Reviews*, *24*(7), 813–819. https://doi.org/10.1016/j.quascirev.2004.07.017

Lipps, J. H., & Krebs, W. N. (1974). Planktonic foraminifera associated with Antarctic sea ice. *Journal of Foraminiferal Research*, *4*, 80–85. https://doi.org/10.2113/gsjfr.4.2.80

Livsey, C. M., Kozdon, R., Bauch, D., Brummer, G. J. A., Jonkers, L., Orland, I., et al. (2020). High-Resolution Mg/Ca and δ^{18}O Patterns in Modern Neogloboquadrina pachyderma From the Fram Strait and Irminger Sea. *Paleoceanography and Paleoclimatology*, *35*, e2020PA003969. https://doi.org/10.1029/2020PA003969

Lund, D. C., Adkins, J. F., & Ferrari, R. (2011). Abyssal Atlantic circulation during the Last Glacial Maximum: Constraining the ratio between transport and vertical mixing. *Paleoceanography*, *26*, 19. https://doi.org/10.1029/2010pa001938

MacGilchrist, G. A., Naveira Garabato, A. C., Brown, P. J., Jullion, L., Bacon, S., Bakker, D. C. E., et al. (2019). Reframing the carbon cycle of the subpolar Southern Ocean. *Science Advances*, *5*(8). https://doi.org/10.1126/sciadv.aav6410

Mackensen, A., Hubberten, H.-W., Scheele, N., & Schlitzer, R. (1996). Decoupling of δ13CΣCO_2 and phosphate in recent Weddell Sea deep and bottom water: Implications for glacial Southern Ocean paleoceanography. *Paleoceanography*, *11*(2), 203–215. https://doi.org/10.1029/95PA03840

Marchitto, T. M., Curry, W. B., Lynch-Stieglitz, J., Bryan, S. P., Cobb, K. M., & Lund, D. C. (2014). Improved oxygen isotope temperature calibrations for cosmopolitan benthic foraminifera. *Geochimica et Cosmochimica Acta*, *130*, 1–11. https://doi.org/10.1016/j.gca.2013.12.034

Martinson, D. G. (1990). Evolution of the Southern Ocean winter mixed layer and sea ice: Open ocean deepwater formation and ventilation. *Journal of Geophysical Research*, *95*(C7), 11641–11654. https://doi.org/10.1029/jc095ic07p11641

Marzocchi, A., & Jansen, M. F. (2019). Global cooling linked to increased glacial carbon storage via changes in Antarctic sea ice. *Nature Geoscience*, *12*(12), 1001–1005. https://doi.org/10.1038/s41561-019-0466-8

Massé, G., Belt, S. T., Crosta, X., Schmidt, S., Snape, I., Thomas, D. N., & Rowland, S. J. (2011). Highly branched isoprenoids as proxies for variable sea ice conditions in the Southern Ocean. *Antartic science*, *23*(5), 487–498. https://doi.org/10.1017/s0954102011000381

Matsumoto, K., Lynch-Stieglitz, J., & Anderson, R. F. (2001). Similar glacial and Holocene Southern Ocean hydrography. *Paleoceanography*, *16*(5), 445–454. https://doi.org/10.1029/2000pa000549

Meilland, J., Schiebel, R., Lo Monaco, C., Sanchez, S., & Howa, H. (2018). Abundances and test weights of living planktic foraminifers across the Southwest Indian Ocean: Implications for carbon fluxes. *Deep Sea Research Part I: Oceanographic Research Papers*, *131*, 27–40. https://doi.org/10.1016/j.dsr.2017.11.004

Metcalfe, B., Feldmeijer, W., & Ganssen, G. M. (2019). Oxygen isotope variability of planktonic foraminifera provide clues to past upper ocean seasonal variability. *Paleoceanography and Paleoclimatology*, *34*(3), 374–393. https://doi.org/10.1029/2018pa003475

Mikis, A., Hendry, K. R., Pike, J., Schmidt, D. N., Edgar, K. M., Peck, V., et al. (2019). Temporal variability in foraminiferal morphology and geochemistry at the West Antarctic Peninsula: A sediment trap study. *Biogeosciences*, *16*(16), 3267–3282. https://doi.org/10.5194/bg-16-3267-2019

Moffat, C., & Meredith, M. (2018). Shelf-ocean exchange and hydrography west of the Antarctic Peninsula: A review. *Philosophical Transactions of the Royal Society A: Mathematical, Physical & Engineering Sciences*, *376*(2122). https://doi.org/10.1098/rsta.2017.0164

Morales Maqueda, M. A., & Rahmstorf, S. (2002). Did Antarctic sea-ice expansion cause glacial CO_2 decline? *Geophysical Research Letters*, *29*(1), 11–13. https://doi.org/10.1029/2001gl013240

Mortyn, P. G., & Charles, C. D. (2003). Planktonic foraminiferal depth habitat and δ^{18}O calibrations: Plankton tow results from the Atlantic sector of the Southern Ocean. *Paleoceanography*, *18*(2). https://doi.org/10.1029/2001pa000637

Naveira Garabato, A. C., McDonagh, E. L., Stevens, D. P., Heywood, K. J., & Sanders, R. J. (2002). On the export of Antarctic bottom water from the Weddell Sea. *Deep Sea Research Part II: Topical Studies in Oceanography*, *49*(21), 4715–4742. https://doi.org/10.1016/s0967-0645(02)00156-x

Norris, R. D., Kim, D. Y., Park, B.-K., Kang, S.-H., & Khim, B.-K. (1998). Stable isotope and ecological habitat of planktonic foraminifera adjacent to the ice edge in the western Weddell Sea. *Journal of Geosciences*, *2*(2), 88–98. https://doi.org/10.1007/bf02910487

O'Neil, J. R., Clayton, R. N., & Mayeda, T. K. (1969). Oxygen isotope fractionation in divalent metal carbonates. *The Journal of Chemical Physics*, *51*(12), 5547–5558.

Orsi, A. H., Johnson, G. C., & Bullister, J. L. (1999). Circulation, mixing, and production of Antarctic bottom water. *Progress in Oceanography*, *43*, 55–109. https://doi.org/10.1016/s0079-6611(99)00004-x

Orsi, A. H., Whitworth, T., III, & Nowlin, W. D., Jr. (1995). On the meridional extent and fronts of the Antarctic circumpolar current. *Deep Sea Research Part I: Oceanographic Research Papers*, *42*(5), 641–673. https://doi.org/10.1016/0967-0637(95)00021-w

Ostermann, D. R., & Curry, W. B. (2000). Calibration of stable isotopic data: An enriched $\delta^{18}O$ standard used for source gas mixing detection and correction. *Paleoceanography*, *15*(3), 353–360. https://doi.org/10.1029/1999pa000411

Park, Y.-H., Charriaud, E., & Fieux, M. (1998). Thermohaline structure of the Antarctic surface water/winter water in the Indian sector of the Southern Ocean. *Journal of Marine Systems*, *17*(1–4), 5–23. https://doi.org/10.1016/s0924-7963(98)00026-8

Peck, V. L., Allen, C. S., Kender, S., McClymont, E. L., & Hodgson, D. A. (2015). Oceanographic variability on the West Antarctic Peninsula during the Holocene and the influence of Upper Circumpolar Deep Water. *Quaternary Science Reviews*, *119*, 54–65. https://doi.org/10.1016/j.quascirev.2015.04.002

Pellichero, V., Sallée, J.-B., Chapman, C. C., & Downes, S. M. (2018). The southern ocean meridional overturning in the sea-ice sector is driven by freshwater fluxes. *Nature Communications*, *9*(1). https://doi.org/10.1038/s41467-018-04101-2

Pellichero, V., Sallée, J.-B., Schmidtko, S., Roquet, F., & Charrassin, J.-B. (2017). The ocean mixed layer under Southern Ocean sea-ice: Seasonal cycle and forcing. *Journal of Geophysical Research: Oceans*, *122*(2), 1608–1633. https://doi.org/10.1002/2016jc011970

Pichon, J.-J., Bareille, G., Labracherie, M., Labeyrie, L. D., Baudrimont, A., & Turon, J.-L. (1992). Quantification of the biogenic silica dissolution in Southern Ocean sediments. *Quaternary Research*, *37*(3), 361–378. https://doi.org/10.1016/0033-5894(92)90073-r

Roemmich, D., & Gilson, J. (2009). The 2004-2008 mean and annual cycle of temperature, salinity, and steric height in the global ocean from the Argo Program. *Progress in Oceanography*, *82*(2), 81–100. https://doi.org/10.1016/j.pocean.2009.03.004

Ryan, W. B. F., Carbotte, S. M., Coplan, J. O., O'Hara, S., Melkonian, A., Arko, R., et al. (2009). Global multi-resolution topography synthesis. *Geochemistry, Geophysics, Geosystems*, *10*, 9. https://doi.org/10.1029/2008gc002332

Sabu, P., Libera, S. A., Chacko, R., Anilkumar, N., Subeesh, M. P., & Thomas, A. P. (2020). Winter water variability in the Indian Ocean sector of Southern Ocean during austral summer. *Deep-Sea Research Part II Topical Studies in Oceanography*, *178*. https://doi.org/10.1016/j.dsr2.2020.104852

Saenko, O. A., Schmittner, A., & Weaver, A. J. (2002). On the role of wind-driven sea ice motion on ocean ventilation. *Journal of Physical Oceanography*, *32*(12), 3376–3395. https://doi.org/10.1175/1520-0485(2002)032<3376:otrowd>2.0.co;2

Schmidtko, S., Johnson, G. C., & Lyman, J. M. (2013). MIMOC: A global monthly isopycnal upper-ocean climatology with mixed layers. *Journal of Geophysical Research: Oceans*, *118*(4), 1658–1672. https://doi.org/10.1002/jgrc.20122

Shackleton, N. (1974). Attainment of isotopic equilibrium between ocean water and the benthonic species Uvigerina: Isotopic changes during the last glacial. *Colloques Internationaux Du CNRS*, *219*, 203–209.

Spindler, M., & Dieckmann, G. S. (1986). Distribution and abundance of the planktic foraminifer Neogloboquadrina pachyderma in sea ice of the Weddell Sea (Antarctica). *Polar Biology*, *5*(3), 185–191. https://doi.org/10.1007/bf00441699

Stephens, B. B., & Keeling, R. F. (2000). The influence of Antarctic sea ice on glacial-interglacial CO_2 variations. *Nature*, *404*(6774), 171–174. https://doi.org/10.1038/35004556

Stössel, A., Kim, S.-J., & Drijfhout, S. S. (1998). The impact of Southern Ocean sea ice in a Global Ocean model. *Journal of Physical Oceanography*, *28*(10), 1999–2018. https://doi.org/10.1175/1520-0485(1998)028<1999:tiosos>2.0.co;2

Sun, X., & Matsumoto, K. (2010). Effects of sea ice on atmospheric pCO_2: A revised view and implications for glacial and future climates. *Journal of Geophysical Research: Biogeosciences*, *115*(G2). https://doi.org/10.1029/2009jg001023

Talley, L. (2013). Closure of the Global Overturning Circulation Through the Indian, Pacific, and Southern Oceans: Schematics and Transports. *Oceanog*, *26*(1), 80–97. https://doi.org/10.5670/oceanog.2013.07

Tan, F. C., & Strain, P. M. (1996). Sea ice and oxygen isotopes in Foxe Basin, Hudson Bay, and Hudson Strait, Canada. *Journal of Geophysical Research*, *101*(C9), 20869–20876. https://doi.org/10.1029/96jc01557

Thomas, E. R., Allen, C. S., Etourneau, J., King, A. C. F., Severi, M., Winton, V. H. L., et al. (2019). Antarctic Sea ice proxies from marine and ice core archives suitable for reconstructing sea ice over the past 2000 years. *Geosciences*, *9*(12), 506. https://doi.org/10.3390/geosciences9120506

Vernet, M., Geibert, W., Hoppema, M., Brown, P. J., Haas, C., Hellmer, H. H., et al. (2019). The Weddell Gyre, Southern Ocean: Present Knowledge and future challenges. *Reviews of Geophysics*, *57*(3), 623–708.

Vorrath, M.-E., Müller, J., Esper, O., Mollenhauer, G., Haas, C., Schefuß, E., & Fahl, K. (2019). Highly branched isoprenoids for Southern Ocean sea ice reconstructions: A pilot study from the Western Antarctic Peninsula. *Biogeosciences*, *16*(15), 2961–2981. https://doi.org/10.5194/bg-16-2961-2019

Watkins, A. B., & Simmonds, I. (1999). A late spring surge in the open water of the Antarctic sea ice pack. *Geophysical Research Letters*, *26*(10), 1481–1484. https://doi.org/10.1029/1999gl900292

Watson, A. J., Vallis, G. K., & Nikurashin, M. (2015). Southern Ocean buoyancy forcing of ocean ventilation and glacial atmospheric CO_2. *Nature Geoscience*, *8*(11), 861–864. https://doi.org/10.1038/ngeo2538

Whitehead, J. M., & McMinn, A. (2002). Kerguelen Plateau Quaternary-late Pliocene palaeoenvironments: From diatom, silicoflagellate and sedimentological data. *Palaeogeography, Palaeoclimatology, Palaeoecology*, *186*, 335–368. https://doi.org/10.1016/s0031-0182(02)00424-8

Whitworth, T., & Nowlin, W. D. (1987). Water masses and currents of the Southern Ocean at the Greenwich Meridian. *Journal of Geophysical Research*, *92*, 6462–6476. https://doi.org/10.1029/jc092ic06p06462

Wilson, E. A., Riser, S. C., Campbell, E. C., & Wong, A. P. S. (2019). Winter upper-ocean stability and ice-ocean feedbacks in the sea ice-covered Southern Ocean. *Journal of Physical Oceanography*, *49*(4), 1099–1117. https://doi.org/10.1175/jpo-d-18-0184.1

Zielinski, U., & Gersonde, R. (1997). Diatom distribution in Southern Ocean surface sediments (Atlantic sector): Implications for paleoenvironmental reconstructions. *Palaeogeography, Palaeoclimatology, Palaeoecology*, *129*(3–4), 213–250. https://doi.org/10.1016/s0031-0182(96)00130-7

References From the Supporting Information

Belanger, P. E., Curry, W. B., & Matthews, R. K. (1981). Core-top evaluation of benthic foraminiferal isotopic ratios for paleo-oceanographic interpretations. *Palaeogeography, Palaeoclimatology, Palaeoecology*, *33*(1–3), 205–220. https://doi.org/10.1016/0031-0182(81)90039-0

Charles, C. D. (1991). *Late Quaternary ocean chemistry and climate change from an Antarctic deep sea sediment perspective (Doctoral dissertation)*. Columbia University.

Charles, C. D., & Fairbanks, R. G. (1990). Glacial to interglacial changes in the isotopic gradients of Southern Ocean surface water. In Geological history of the polar oceans: Arctic versus Antarctic.

Charles, C. D., & Fairbanks, R. G. (1992). Evidence from Southern Ocean sediments for the effect of North Atlantic deep-water flux on climate. *Nature*, *355*(6359), 416–419. https://doi.org/10.1038/355416a0

Charles, C. D., Froelich, P. N., Zibello, M. A., Mortlock, R. A., & Morley, J. J. (1991). Biogenic opal in Southern Ocean sediments over the last 450,000 years: Implications for surface water chemistry and circulation. *Paleoceanography*, *6*(6), 697–728. https://doi.org/10.1029/91pa02477

Charles, C. D., Lynch-Stieglitz, J., Ninnemann, U. S., & Fairbanks, R. G. (1996). Climate connections between the hemisphere revealed by deep sea sediment core/ice core correlations. *Earth and Planetary Science Letters*, *142*(1–2), 19–27. https://doi.org/10.1016/0012-821x(96)00083-0

Curry, W. B., Duplessy, J. C., Labeyrie, L. D., & Shackleton, N. J. (1988). Changes in the distribution of δ13C of deep water ΣCO_2 between the Last Glaciation and the Holocene. *Paleoceanography*, *3*, 317–341. https://doi.org/10.1029/pa003i003p00317

Duplessy, J. C., Labeyrie, L., Paterne, M., Hovine, S., Fichefet, T., Duprat, J., & Labracherie, M. (1996). High latitude deep water sources during the last glacial maximum and the intensity of the global oceanic circulation. In G. Wefer, et al. (Eds.), *The South Atlantic: Present and past circulation* (pp. 445–460). Springer-Verlag. https://doi.org/10.1007/978-3-642-80353-6_24

Duplessy, J.-C., Shackleton, N. J., Matthews, R. K., Prell, W., Ruddiman, W. F., Caralp, M., & Hendy, C. H. (1984). 13C record of benthic foraminifera in the last interglacial ocean: Implications for the carbon cycle and the global deep water circulation. *Quaternary Research*, *21*(2), 225–243. https://doi.org/10.1016/0033-5894(84)90099-1

Graham, D. W., Corliss, B. H., Bender, M. L., & Keigwin, L. D., Jr. (1981). Carbon and oxygen isotopic disequilibria of recent deep-sea benthic foraminifera. *Marine Micropaleontology*, *6*(5–6), 483–497. https://doi.org/10.1016/0377-8398(81)90018-9

Greco, M., Jonkers, L., Kretschmer, K., Bijma, J., & Kucera, M. (2019). Depth habitat of the planktonic foraminifera Neogloboquadrina pachyderma in the northern high latitudes explained by sea-ice and chlorophyll concentrations. *Biogeosciences*, *16*(17), 3425–3437. https://doi.org/10.5194/bg-16-3425-2019

Grobe, H., & Mackensen, A. (1992). Late Quaternary climatic cycles as recorded in sediments from the Antarctic continental margin. *Antarctic Research Series - American Geophysical Union*, *56*, 349–376.

Grobe, H., Mackensen, A., Hubberten, H.-W., Spiess, V., & Futterer, D. K. (1990). Stable isotope record and Late Quaternary sedimentation rates at the Antarctic continental margin. In *Geological history of the polar oceans: Arctic versus Antarctic*. Dordrecht, Springer. https://doi.org/10.2973/odp.proc.sr.113.193.1990

Hodell, D. A. (1993). Late Pleistocene Paleoceanography of the South Atlantic Sector of the Southern Ocean: Ocean Drilling Program Hole 704A. *Paleoceanography*, *8*(1), 47–67. https://doi.org/10.1029/92pa02774

Keigwin, L. D., & Boyle, E. A. (1989). Late quaternary paleochemistry of high-latitude surface waters. *Palaeogeography, Palaeoclimatology, Palaeoecology*, *73*(1–2), 85–106. https://doi.org/10.1016/0031-0182(89)90047-3

Key, R. M., Kozyr, A., Sabine, C. L., Lee, K., Wanninkhof, R., Bullister, J. L., et al. (2004). A global ocean carbon climatology: Results from Global Data Analysis Project (GLODAP). *Global Biogeochemical Cycles*, *18*(4), 23. https://doi.org/10.1029/2004gb002247

Mackensen, A., Grobe, H., Hubberten, H., & Kuhn, G. (1994). Benthic foraminiferal assemblages and the d13C signal in the Atlantic sector of the Southern Ocean: Glacial-to-interglacial contrasts. In R. Zahn (Ed.), *Carbon cycling in the glacial ocean. Constraints on the ocean's role in global change* (pp. 587–610). Berlin, Heidelberg: Springer.

Mackensen, A., Grobe, H., Hubberten, H.-W., Spiess, V., & Fütterer, D. K. (1989). Stable isotope stratigraphy from the Antarctic continental margin during the last one million years. *Marine Geology*, *87*(2–4), 315–321. https://doi.org/10.1016/0025-3227(89)90068-6

Mackensen, A., Hubberten, H.-W., Bickert, T., Fischer, G., & Fütterer, D. K. (1993). The δ13C in benthic foraminiferal tests of Fontbotia wuellerstorfi (Schwager) Relative to the δ13C of dissolved inorganic carbon in Southern Ocean Deep Water: Implications for glacial ocean circulation models. *Paleoceanography*, *8*(5), 587–610. https://doi.org/10.1029/93pa01291

Mackensen, A., Rudolph, M., & Kuhn, G. (2001). Late pleistocene deep-water circulation in the subantarctic eastern Atlantic. *Global and Planetary Change*, *30*(3–4), 197–229. https://doi.org/10.1016/s0921-8181(01)00102-3

Meier, W., Fetterer, M., Savoie, M., Mallory, S., Duerr, R., & Stroeve, J. (2017). *NOAA/NSIDC climate data record of passive microwave sea ice concentration, version 3*. National Snow and Ice Data Center.

Niebler, H. (1995). Reconstruction of paleo-environmental parameters using stable isotopes and fanual assemblages of planktonic foraminifera in the Southern Atlantic Ocean. *Polarforschung*, *167*, 1–198.

Niebler, H. (2004). d18O of Neogloboquadrina pachyderma in surface sediments. *PANGAEA*. https://doi.org/10.1594/PANGAEA.55866

Ninnemann, U. S., & Charles, C. D. (2002). Changes in the mode of Southern Ocean circulation over the last glacial cycle revealed by foraminiferal stable isotopic variability. *Earth and Planetary Science Letters*, *201*(2), 383–396. https://doi.org/10.1016/s0012-821x(02)00708-2

Ott, G., & Gersonde, R. (1997). *Sedimentology and stable isotopes on core PS1649-2*. https://doi.org/10.1594/PANGAEA.5177010.1007/978-3-322-99410-3

Peng, G., Meier, W. N., Scott, D. J., & Savoie, M. H. (2013). A long-term and reproducible passive microwave sea ice concentration data record for climate studies and monitoring. *Earth System Science Data*, *5*(2), 311–318. https://doi.org/10.5194/essd-5-311-2013

Pöppelmeier, F., Gutjahr, M., Blaser, P., Keigwin, L. D., & Lippold, J. (2018). Origin of Abyssal NW Atlantic water masses since the last glacial maximum. *Paleoceanography and Paleoclimatology*, *33*(5), 530–543. https://doi.org/10.1029/2017pa003290

Sarnthein, M., Winn, K., Duplessy, J.-C., & Fontugne, M. R. (1988). Global variations of surface ocean productivity in low and mid latitudes: Influence on CO_2 reservoirs of the Deep Ocean and atmosphere during the last 21,000 years. *Paleoceanography*, *3*(3), 361–399. https://doi.org/10.1029/pa003i003p00361